University of São Paulo
"Luiz de Queiroz" College of Agriculture

Genesis and organic matter chemistry of sombric horizons in subtropical soils (Paraná State, Brazil)

Mariane Chiapini

Thesis presented to obtain the degree of Master in Science. Area: Soil and Plant Nutrition

Piracicaba
2017

Mariane Chiapini
Agronomist

Genesis and organic matter chemistry of sombric horizons in subtropical soils (Paraná State, Brazil)

versão revisada de acordo com a resolução CoPGr 6018 de 2011

Advisor:
Prof. Dr. **PABLO VIDAL TORRADO**

Thesis presented to obtain the degree of Master in Science. Area: Soil and Plant Nutrition

Piracicaba
2017

Dados Internacionais de Catalogação na Publicação
DIVISÃO DE BIBLIOTECA – DIBD/ESALQ/USP

Chiapini, Mariane

Genesis and organic matter chemistry of sombric horizons in subtropical soils (Paraná State, Brazil)/ Mariane Chiapini.- - versão revisada de acordo com a resolução CoPGr 6018 de 2011. - - Piracicaba, 2017.

66 p.

Dissertação (Mestrado) - - USP / Escola Superior de Agricultura "Luiz de Queiroz".

1. Pirólise-CG/EM 2. Composição isotópica ($\delta^{13}C$) 3. Black carbon 4. Reconstrução Paleoambiental. I. Título

ACKNOWLEDGMENTS

My sincere gratitude to Prof. Dr. Pablo Vidal Torrado, my adviser, to incentive, support, trust, knowledge transmitted, friendship and above all for the patience.

I am very grateful also to Drª Judith Schellekens by teaching and knowledge transmitted, great collaboration, suggestions, trust, friendship and patience.

I would like to thank the Graduate Program in Soils and Plant Nutrition and the Soil Science Department from ESALQ/USP for the opportunity of taking the course and for the availability of the facilities, resources and materials for the development of my research work.

I thank the São Paulo Research Foundation (FAPESP) and CAPES for the regular master scholarship.

Thanks Dr. Jaime Antônio de Almeida, Dr. Márcia Regina Calegari and Dr. Plínio Barbosa de Camargo for teachings and laboratory analysis.

Thanks to my friends of the graduate program Danilo, Gabriel Nuto, Lucas, Karina, Ana Bárbara, Sara, Murilo, Beatriz and those already concluded Rodrigo, Josiane, Jairo, Gabriel, Raphael, Pedro, Marina, Taís, José Ricardo, Alexandre by collaboration, fellowship, laughter and incentives.

Thanks to my friend's house (Virginetes) for the friendship, knowledge, parties and incentive.

Thanks to teachers of the Soil Science Department - ESALQ/USP by the knowledge transmitted and contribution to my education.

I thank Luiz Silva, Nivanda, Sônia, Chiquinho, Leandro and Rossi the technicians of the Soil Science Department - ESALQ/USP for the attention and support in laboratory analyses.

Thanks to employees of the Soil Science Department - ESALQ/USP, Dorival Grisotto, Marta, Cristina, Célia, Sueli, Martinha.

Special thanks to my family, Carlos, Marinalva, my brother Frederico and my boyfriend Bruno by the unconditional love and encouraging the pursuit of my goals.

To all the people who contributed directly or indirectly to this research.

Thank you!

CONTENTS

RESUMO

Gênese e química da matéria orgânica de horizontes sômbricos em solos subtropicais (Paraná, Brasil)

A matéria orgânica do solo (MOS) desempenha um papel importante no ciclo global do carbono. Portanto, é importante entender a estabilidade da MOS, que está relacionada a vários processos. As suas propriedades intrínsecas podem estar relacionadas com a sua estabilidade, por exemplo, o "black carbon" é considerado relativamente resistente à degradação. Na maioria dos solos, os horizontes escuros coincidem com as camadas ou horizontes superficiais devido ao maior acúmulo de matéria orgânica, mas nos estados do sul do Brasil, a presença de solos com horizontes subsuperficiais escurecidos é frequentemente observada. O horizonte subsuperficial escurecido destes solos assemelha-se a um horizonte sômbrico. Aspectos sobre sua origem, formação e preservação ainda não foram totalmente elucidados. O objetivo deste trabalho é compreender a formação de horizontes 'sômbricos' em solos da região de Tijucas do Sul (Paraná, Brasil). Foram descritos e coletados cinco perfis de solo, dos quais três estão localizados em uma topossequência e continham um horizonte similar ao sômbrico (P1-P3), um solo de referência representativo da área (P5) e um solo intermediário (P4) que apresentou uma morfologia entre o solo de referência e os solos com horizonte 'sômbrico'. Para este fim, a MOS foi estudada pela sua composição molecular através da técnica de pirólise acoplada à cromatografia gasosa e espectrometria de massa (pirólise-GC-MS). Além disso, estudou-se a composição isotópica ^{13}C ($\delta^{13}C$) e a composição fitolítica, a fim de compreender as condições paleoclimáticas que foram relacionados com as condições ambientais passadas usando técnicas de datação com ^{14}C, e suportados pelas análises clássicas de solo. As amostras dos horizontes foram submetidas ao fracionamento químico MOS, gerando duas frações: fração extraível com NaOH (EXT) e resíduo (RES). A morfologia dos perfis mostrou uma intensa atividade biológica nos horizontes A e uma ampla distribuição de microfragmentos de carvão. Observou-se também a continuidade lateral de horizontes 'sômbricos' em solos da topossequência (P1-P3), diferenciando-os dos horizontes A enterrados. A distribuição da MOS nas frações estudadas pela pirólise foi a mesma para os cinco perfis: EXT> RES. Os produtos relacionados a incêndios florestais como os poliaromáticos (PAHs, BC) foram encontrados em todos os perfis, mas em maior abundância relativa nos horizontes sômbricos, indicando uma maior incidência de incêndio durante a formação destes horizontes. Os PAHs podem estar relacionados com a manutenção da cor escura dos horizontes 'sômbricos'. Em relação às condições paleoclimáticas observou-se que os horizontes subsuperficiais escurecidos foram desenvolvidos durante o Holoceno Médio sob vegetação composta principalmente por gramíneas C_4 com arbustos, evidenciando um clima mais seco correspondente a maior incidência de incêndio.

Palavras-chave: Pirólise-CG/EM; Composição isotópica ($\delta^{13}C$); Black carbon; Reconstrução paleoambiental

ABSTRACT

Genesis and organic matter chemistry of sombric horizons in subtropical soils (Paraná State, Brazil)

Soil organic matter (SOM) plays an important role in the global carbon cycle. Therefore, it is important to understand the stability of SOM, which is related to several processes. Its intrinsic properties may be related to its stability, for example black carbon is considered to be relatively resistant to degradation. In most soils, the dark horizons coincide with the superficial layers or horizons due to the greater accumulation of organic matter, but in the southern states of Brazil, the presence of soils with dark subsurface horizons is frequently observed. The dark subsurface horizon of these soils are similar to a sombric horizon. Aspects about its origin, formation and preservation have not yet been fully elucidated. The objective of this work is to understand the formation of 'sombric' horizons in soils of the region fromTijucas do Sul (Paraná, Brazil). Five soil profiles were described and collected, from which three originate from a toposequence and contained a 'sombric' horizon (P1–P3), a reference soil that is representative of the area (P5) and an intermediate soil (P4) that showed morphology between the reference soil and the soils with a 'sombric' horizon. To this end SOM is studied for its molecular composition by the pyrolysis technique coupled to gas chromatography and mass spectrometry (pyrolysis-GC-MS). In addition, ^{13}C isotopic composition ($\delta^{13}C$) and phytolytic composition were studied in order to understand paleoclimatic conditions. These results will be related to past environmental conditions using ^{14}C dating techniques, and supported by classical soil analysis. The samples of the horizons were submitted to the SOM chemical fractionation, generating two fractions: extractable fraction with NaOH (EXT) and residue (RES). The morphology of the profiles showed an intense biological activity in A horizons and a wide distribution of microfragments of charcoals. The lateral continuity of 'sombric' horizons in toposequence soils was also observed, which differentiated them (P1-P3) from buried A horizons. The distribution of SOM in the fractions studied was the same for the five profiles studied: EXT> RES. Products related to wildfires such as polyaromatics (PAHs; BC) were found in all profiles, but in greater relative abundance in the 'sombric' horizons, indicating a higher incidence of fire during the formation of these horizons and these compounds can be related to the maintenance of dark color of the 'sombric' horizons. In relation to the paleoclimatic conditions it was observed that the dark subsurface horizons were developed during the Mid-Holocene under vegetation composed mainly by C_4 grasses with shrubs, evidencing a drier climate corresponding to a higher fire incidence.

Keywords: Pyrolysis-GC/MS; $\delta^{13}C$ isotopic composition; Black carbon; Paleoenvironmental reconstruction

1. INTRODUCTION

The soil organic matter (SOM) contains about three times more carbon than the atmosphere and terrestrial vegetation (Schmidt et al., 2011), being an important carbon source to atmosphere. Therefore, it is important to understand the stability of soil organic matter and about the characteristics of paleoenvironmental conditions. According to Klotzbücher et al. (2011) the stability of SOM or decomposition rate is controlled by: a) differences in molecular structure; and b) resistance to transformation of plant macromolecules. Another important factor is the pyrogenic carbon (black carbon - BC) (Schmidt et al., 2011) that is highly resistant to decomposition because of the aromatic rings in their structure and the macromolecular rearrangement caused by fire (Knicker, 2011). However, external factors such as pH, moisture, temperature, redox conditions, availability of nutrients, oxygen, microorganisms and also by intrinsic factors to the organic material such as the C/N ratio and amount of recalcitrant molecules may differ between species and parts of plants. Even do, during the SOM decomposition physical and chemical alterations can happen as well as stabilization. The stabilization of SOM protects it the losses by leaching and erosion. According to Six et al. (2002) and Sollins et al. (1996) it is connected to the following mechanisms: a) chemical recalcitrance; b) adsorption of organic material in the surface of clay minerals; and c) physical protection.

Generally, SOM is observed in surface horizons, but in the southern region of Brazil, this is common in subsurface horizons (Almeida et al., 2015). The formation of these horizons is not well known, but they show a similar morphology with sombric horizons, which are described from Oxisols and Ultisols of the high-altitude areas of Central Africa (Caner et al., 2003; Frankart, 1983). According to Soil Taxonomy (Soil Survey Staff, 2014) and World Reference Base for Soil Resources (WRB-FAO, 2014) the sombric horizon is considered it as a horizon with illuvial humus that is not associated with aluminum (such as in spodic horizons) neither with sodium (such as in natric horizons). Several theories for the genesis of the sombric horizons have been proposed. According to Sys et al. (1961) sombric horizon is formed by the illuviation of organic compounds. Studying Andean soils of Colombia, Faivre (1990) proposed that the sombric horizons are a result of migration and precipitation of clay-humic complexes, while Caner et al. (2003) proposed that the genesis of these horizons in India are related to a vegetation changes and origin of SOM caused by a climatic changes in the past.

Knowing this and the possible genesis of the dark subsurface horizon cited above could be hypothesized that de darkening of color observed in soil profiles of Tijucas do Sul can be related to: a) changes in the nature of the OM from the surface horizon induced by climatic changes with persistence of more stable OM in the subsurface, like a BC (Caner et al., 2003; Velasco-Molina et al., 2013); b) humus have been transported and accumulated in these horizons in combination with clay or similar fraction in form of OM-metal complexes like in Podzolization process (Faivre, 1990: Almeida et al., 2009, 2015).

So, in order to understand the formation of dark subsurface horizons, the factors that control the stability of SOM and a possible climatic change, a qualitative characterization of the OM of the soil profiles of Tijucas do Sul it is important. For this, the pyrolysis-gas chromatography-mass spectrometry (Py-GC-MS) was chosen to study the molecular composition of SOM in combination with classical soil analyzes (micromorphology, mineralogy, chemical and physical) and specific analysis for paleoenvironmental reconstruction (phytoliths, $\delta^{13}C$ isotopic composition and ^{14}C datings). The pyrolysis GC-MS is a technique that provides detailed information about the molecular composition and origin of organic materials (Buurman et al, 2012; Carr et al, 2013; Derenne et al., 2015; Nierop et al., 2001; Schellekens et al, 2011, 2013). This powerful molecular information is used to compare the molecular composition of organic matter from different soils, different horizons of a given soil profile, different fractions resulting from physical or chemical separations and changes in relation to land management, carbon stability and influence of fire materials (black carbon) in the history of soil (Derenne et al., 2015). Even do, the use of phytoliths, $\delta^{13}C$ isotopic composition and ^{14}C datings analysis are important for characterization of past and current plants present in soil profiles studied here, as well as the climatic conditions can be reconstructed, because these techniques are a powerful paleoenvironmental interpretation and reconstruction (Calegari, 2013a; Oliveira 2014; Paisani et al., 2013b; 2014; Pessenda et al., 1996b).

2. MATERIALS AND METHODS

2.1. Study area and sampling

The study area is located in Tijucas do Sul (Paraná, Brazil; 25°55'41"S, 49°11'56"W) (Figure 1). The parent material of soils in this study seems to be a residuum and a deep colluvium derived mainly from migmatites with local influence of other metamorphic rocks (Santos et al., 2006). The native vegetation is classified as a mosaic of mixed ombrophilous forest which have significant occurrence of *Araucaria* trees and grassland. The climate is temperate and humid (Cfb, Köppen classification) subtropical with a mean annual precipitation of 2000 mm and a mean annual temperature of 22 °C (Behling, 2001).

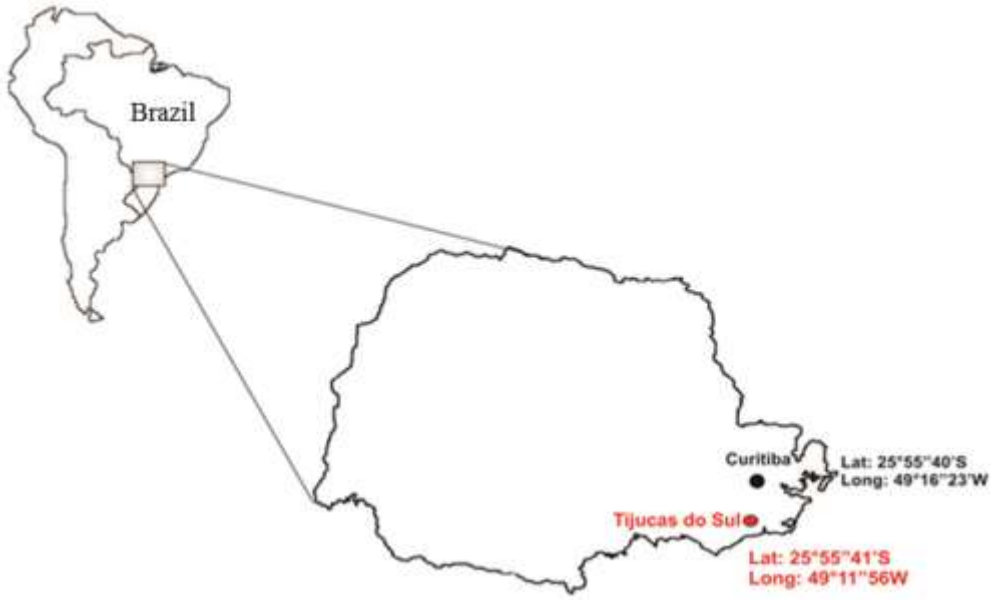

Figure 1. Localization of study area.

The sampled profiles are located at about 950 m a.s.l. and included three pedons with a dark subsurface horizon which is similar to a sombric horizon. The soil profiles were classified as Sombric Nitisol humic (WRB-FAO, 2014; P1–P3). These pedons were situated in a toposequence, with P1 on the summit of a hill, P2 on the upper backslope 58 m downwards, and P3 in lower backslope at a distance of 30 m from P2. A reference soil (P5) was located a distance of 2 km from the toposequence, in the lower backslope of other hill, and was classified as an Abruptic Acrisol humic. In addition, an intermediate soil was sampled (P4); this profile was situated on the summit of the hill from profile P5, and was classified as Sombric Nitisol humic and seemed an intermediate between the 'sombric' and reference soils based on morphology of the dark subsurface horizon. The five profiles were

sampled according to pedogenic horizons as determined in the field according to Santos et al. (2013) and Schoeneberger et al. (2002), resulting in a total of 54 samples. Most analysis was done using these samples. However, for isotope analysis, profiles P1, P4 and P5 were additionally sampled at regular depths at 5 cm intervals and for phytoliths analysis sampled at regular depths at 10 cm intervals until 140 cm of death. Photographs of all five profiles are given in Figure 2. The samples were air-dried and sieved through 2 mm for laboratory analysis.

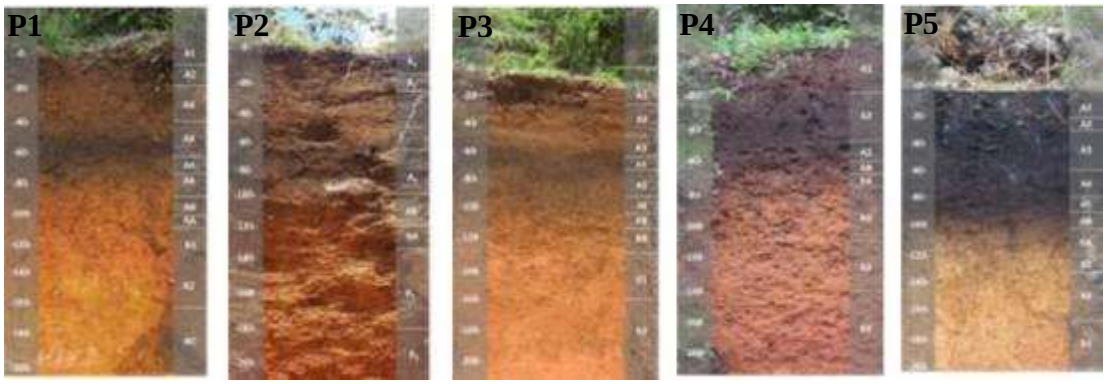

Figure 2. The five pedons of this study.

2.2. General chemical and physical soil characteristics

Chemical analysis included pH (H_2O), Ca^{2+}, Mg^{2+} and Al^{3+}exchangeable by KCl 1 M, H and Al by calcium acetate at pH= 7; P, K^+ and Na^+ by Mehlich; Organic carbon (C_{org}) was determined by wet oxidation with potassium dichromate ($K_2Cr_2O_7$) 0.4 mol L^{-1} (Walkley Black) (Embrapa, 2011). Cation exchange capacity (CEC) was calculated by sum of the exchangeable cations at pH= 7: ((Ca^{2+}, Mg^{2+}, K^+) plus H^+ + Al).

The clay fraction was determined by the hydrometer method (Embrapa, 2011). The sand fraction was sieved and classified into five fractions: very coarse sand (2–1 mm), coarse sand (1–0.5 mm), medium sand (0.5–0.25 mm), fine sand (0.25–0.10 mm) and very fine sand (0.10–0.05 mm). The silt fraction was calculated by subtraction, i.e., silt fraction = 100 – (sand fraction + clay fraction).

X-ray fluorescence spectroscopy was used in bulk samples to quantify some elements (Ti, Zr; to detected eventual soil discontinuities). The equipment was Epsilon 3 of the Panalitical that was located in a mineralogy laboratory at State University of Santa Catarina (UDESC) - Lages Campus.

Ten samples were analyzed by x-ray diffraction (XRD; Jackson, 1979; Kämpf and Schwertmann, 1982), including four samples from dark subsurface horizons, one from an A horizon and five from B horizons. The equipment was a XRD Rigaku Miniflex II with CuKa radiation (λ = 0,154 nm) worked at 10 mA and 15kV. This analysis aims to characterize the mineralogy of the soil profiles and identify differences between them.

2.3. Dithionite, oxalate and pyrophosphate extractable Fe and Al

Different forms of Fe and Al were determined. Extraction with ammonium oxalate solution (Fe_o and Al_o) was done at pH 3.0 in the dark, and extracts most of the amorphous materials (Schwertmann, 1964). Extraction with dithionite-citrate- bicarbonate (Fe_d and Al_d, Mehra & Jackson, 1960) extracts large proportion of the crystalline (pedogenics oxides – hematite and goethite) as well as the amorphous materials. Extraction with 0.1 M sodium pyrophosphate (Fe_p and Al_p) was done at pH 10 according to USDA (1996) and can provides the Fe and Al that is bound to OM.

2.4. Phytoliths

The samples used to study phytoliths were collected at regular intervals of 10 cm, with the aim to identify the past vegetation composition. First of all, the organic matter and iron oxides were removed according to Mehra and Jackson (1960). Then, the separation of phytoliths was carried out with sodium polytungstate (Madella et al., 1998; Calegari et al., 2013). Samples were mounted on slides and they were counted phytoliths. The phytoliths were identified according to International Code for Phytolith Nomenclature - ICPN 1.0 (Madella et al., 2005).

2.5. Micromorphology

In order to investigate possible organic, clay or organic-clay coatings and the presence of charcoal fragments in soils, seventeen undisturbed soil samples were collected from different horizons and transitions within the profiles for micromorphological

descriptions and analysis. Thin 5 x 9 cm sections were prepared and described according to Bullock et al. (1985) and Castro et al. (2003).

2.6. ^{14}C datings

Because no macroscopic charcoal was found in the dark subsurface horizon and B horizons of the soil profiles, the humin fraction was used for ^{14}C dating. This means that instead of absolute ages, the datings reflect mean residence times. Humin of twelve samples was separated according to Pessenda et al. (1996b). ^{14}C analysis was carried out at the Radiocarbon Laboratory (Centro de Energia Nuclear na Agricultura, CENA and the AMS Laboratory at University of Georgia, USA). ^{14}C ages were expressed and calibrated in years before present (2δ).

2.7. Soil OM

2.7.1. Soil OM fractionation

Ten grams of air dried fraction were extracted with 100 ml 0.1 M NaOH and shaken for 18h. The suspensions were centrifuged for 30 min at 8000 rpm and decanted to collect the extracts. This process was repeated until the supernatant remained colorless after centrifuging (four times) and the extracts were combined. The combined extracts (NaOH extracts) were acidified to pH 1–2 with 1 M HF/HCl (3:1) and 15 ml of HF was added, and shaken for 18h. To remove excess salt, the extracts were dialyzed against ultrapure demineralized water in cellulose acetate dialysis tubes with a cut off of 6000 Da, and freeze-dried.

The residue after NaOH extraction was shaken for 18h with a solution of 100 ml 0.1 M sodium pyrophosphate ($Na_4P_2O_7$; Nierop et al., 2005). The suspensions were centrifuged for 30 min at 8000 rpm and decanted to collect the extracts. Because of the colorless extract, this process was not repeated. Similar to the NaOH extracts, the $Na_4P_2O_7$ extracts were acidified, dialyzed, and freeze-dried.

The soil residue after $Na_4P_2O_7$ extraction was oven-dried at 40 °C, from which 1 g was collected for total C and N analysis. Thereafter, this residue was shaken with 30 ml 1 M HF/HCl (3:1). The suspension was centrifuged for 30 min at 8000 rpm and the supernatant was discarded. This step was repeated seven times to remove reactive minerals (Zegouagh et al., 2004). The residue was shaken for two hours with 30 ml 1 M HCl, leaving standing

overnight and washed with distilled water. The final residue was dried at 40 °C and homogenized.

This sequential fractionation was used to separate the fractions of OM with different binding affinity in the studied soils. The NaOH extractable OM is comparable with the combined operationally defined humic and fulvic acid fractions (Leinweber and Schulten, 1999), representing small fragments (< 0,45 µm) that are water soluble and/or weakly bound to mineral surfaces. The $Na_4P_2O_7$ extract was expected to contain OM in metal-organic complexes (Nierop et al., 2005). The residue, after both extractions, contains OM that was not extractable with 0.1 M NaOH nor with 0.1 M $Na_4P_2O_7$, and may include i) strongly mineral bound OM, ii) OM > 0,45 µm and iii) hydrophobic material, or a combination of these characteristics (Knicker et al., 2005; Schellekens et al., 2013, 2016; Wattel-koekkoek et al., 2001). The fractionation scheme is given in Figure 3. For all samples, the color of the $Na_4P_2O_7$ extract was transparent; therefore, only the NaOH extract (EXT) and residue (RES) were analyzed with pyrolysis-GC/MS.

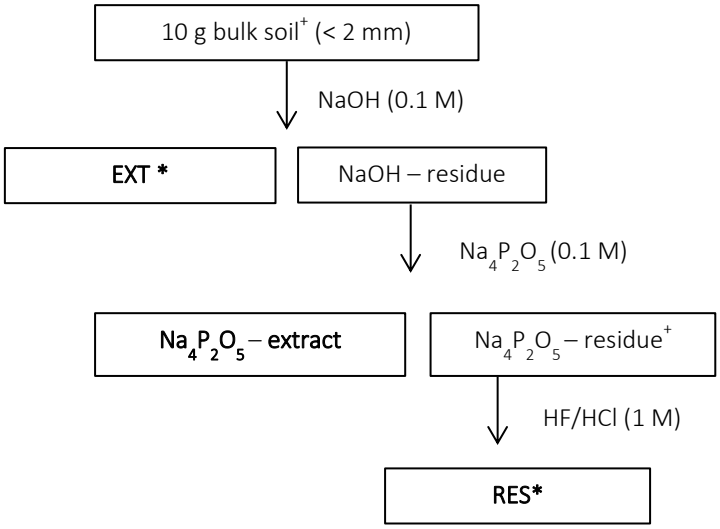

Figure 3. SOM fractionation scheme.

2.7.2. Total C and total N, and $\delta^{13}C$ isotopic composition

Total carbon (C_t) and total nitrogen (N_t) were determined by dry combustion. The equipment was a CN elemental analyzer coupled to an ANCA-SL mass spectrometer 2020 Scientific Europe in Stable Isotope Laboratory of CENA USP. Total C was analyzed for bulk

samples (C_t) and for the RES fraction (C_{RES}; Fig. 2). The total C and N of EXT were obtained through the difference between bulk and RES ($C_{EXT} = C_t - C_{RES}$), which may result in some overestimation of the RES. $\delta^{13}C$ isotopic composition was determined with the same equipment using bulk samples from profiles P1, P4 and P5 (collected with a sample resolution of 5 cm; Section 2.1).

2.7.3. Pyrolysis-GC/MS

Pyrolysis was performed at the Department of Soil Science from ESALQ/USP (Piracicaba, Brazil) using a single shot PY-3030S pyrolyser (Frontier Laboratories, Fukushima, Japan) coupled to a GCMS-QP2010 (Shimadzu, Kyoto, Japan). The pyrolysis temperature was set at 600 °C (+/−0.1 °C); Helium was used as carrier gas at a constant flow of 34.5 ml min^{-1}. The injection temperature of the GC (split 1:20) and the GC-MS interface were set at 320 °C. The GC oven was heated from 50 to 320 °C (held 10 min) at 7 °C min^{-1}. The GC instrument was equipped with an Rtx-5MS column (RESTEK), length 30 m, thickness 0.25 mm, diameter 0.25 μm. The MS was scanning in the range of *m*/*z* 45–600. Pyrolysis products were identified using the NIST '14 mass spectral library and literature (Schellekens et al., 2013; Vancampenhout et al., 2015).

Both EXT and RES were analyzed for all 35 samples resulting in a total of 70 pyrograms. About 900 pyrolysis products were identified, of which 115 products were quantified (Appendix A). The products were grouped according to chemical similarity into a number of source groups: *n*-alkanes ($C_{20} - C_{25}$), branched alkenes, alkylbenzenes, diterpenes, polycyclic aromatic hydrocarbons (PAHs), benzofurans, aromatics, phenols, lignin phenols, N-containing compounds, and polysaccharides. Quantification was based on the peak area of characteristic fragment ions (*m/z* values) for each pyrolysis product. All quantification was checked manually. For each sample, the sum of the quantified peak areas, expressed as total ion current (TIC), was set at 100% and relative amounts were calculated with respect to this sum. The resulting quantification allows a reliable comparison of the relative abundance of each pyrolysis product within a set of samples.

2.8. Data analysis

In order to identify lithologic discontinuities (LDs) in the studied soil profiles, many indexes have been used. Schatzel (1998) found that the uniformity value (UV) was the most

useful parameter to identify LDs. Furthermore, the distribution of the Ti/Zr ratio and the sand/silt ratio was used too. The UV was calculated according to Cremeens and Mokma (1986) and Schatzel (1998) comparing particle-size data in the upper horizon and lower horizon.

Factor analysis was performed on the quantified phytoliths and pyrolysis products with Statistica software, version 6 (Statsoft). Factor analysis was applied to pyrolysates from all soil samples (A–BA horizons) (EXT and RES) to provide an indication of the main chemical differences, between the fractions, profiles and/or depth. Sample resolution for phytoliths and $\delta^{13}C$ isotopic analysis differed compared to other analysis, and had a higher resolution (10 cm for phytoliths, 5 cm for isotopes) and lower number of profiles (P1, P4 and P5). Statistical comparison with pyrolysis data is therefore presented, and depth records were used to compare the different sample sets. Factor analysis was used to extract the main differences/changes in phytolith composition between profiles and with depth. Depth records of the factor scores were used for comparison with molecular proxies and $\delta^{13}C$ isotopic composition.

3. RESULTS AND DISCUSSION

3.1. Soil morphology, micromorphology, classification and general characteristics

The profiles of the toposequence (P1, P2 and P3) and profile P4 were characterized by the presence of a dark subsurface horizon which was classified like a ‘sombric’ horizon in P1–P3. The depth of this horizon ranged between 50 and 95 cm. The ‘sombric’ horizon presented color differences in relation to the epipedons and its lateral configuration follows the topography of the slope in several parts of the local landscape (Figure 4), which distinguish them from a buried A horizon. The color of these dark horizons varied from dark reddish brown (5YR 3/2, moist) in P1 to black (7,5YR 2.5/1, moist) in P2 and P3, as well as a lower color value and chroma in relation to epipedons (Table 1; Figure 2). These color differences are in agreement with those found by Caner et al. (2003) in sombric-like subsurface A horizons from India. Apart from the absence of this dark subsurface horizon, the reference soil (P5) showed some additional morphologic differences, including the presence of an O horizon, as well as a hyperhumic horizon (FAO, 2014). The colors of the epipedons in profile P5 were homogenously until 90 cm depth, being black (7.5YR 2.5/1) according to the Munsell soil-color chart.

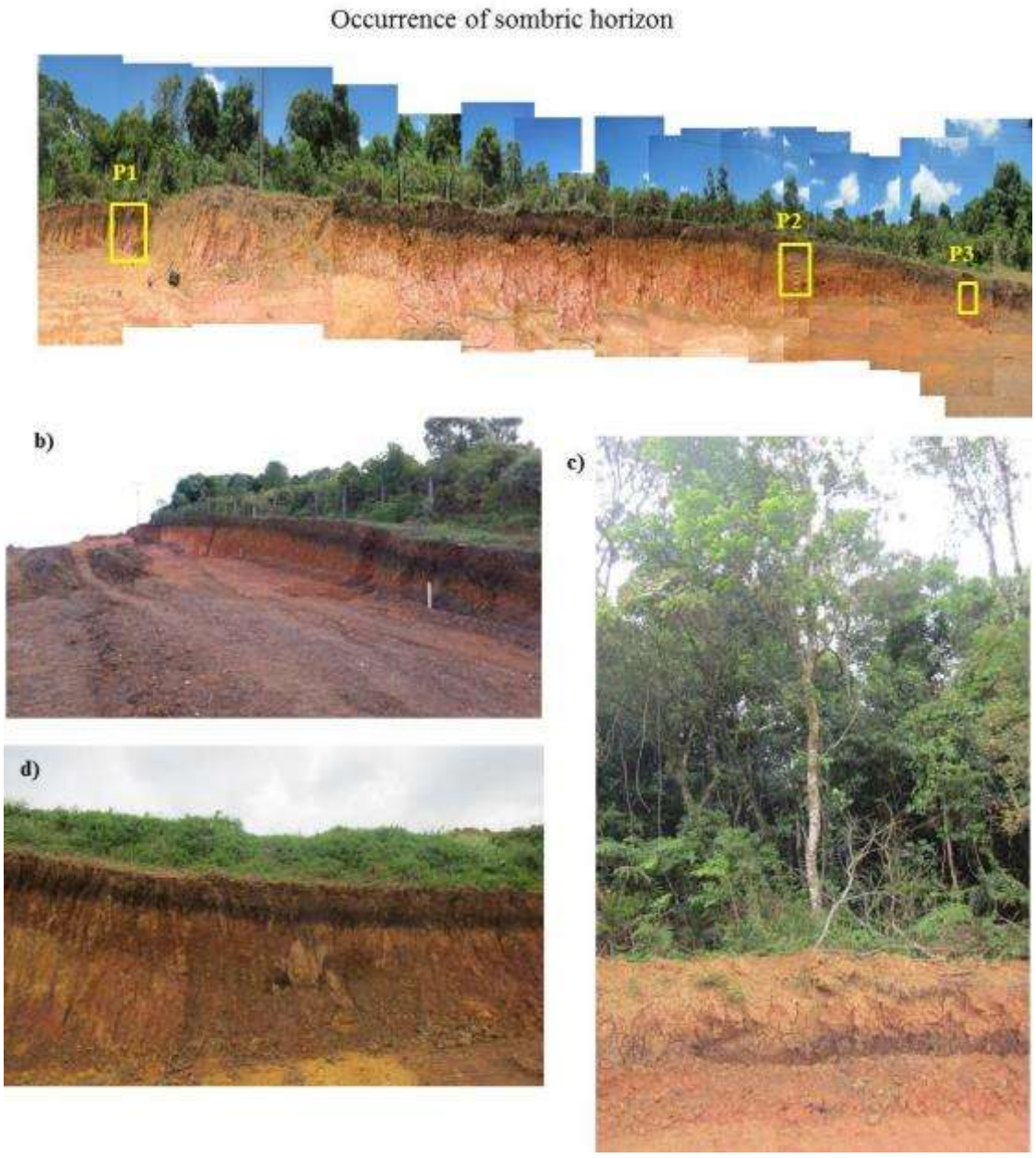

Figure 4. Occurrence of sombric horizon in the region of the studied soil profiles. a) Photographic composition of the soils of the toposequence (P1-P3), observe the sombric horizon; b) Lateral configuration of the sombric horizon (subsurface dark horizon); c) and d) Sombric horizon a nearby area.

Table 1. General properties of the studied soil profiles.

Pedon	Horizon	Depth (cm)	Colour (moist)	pH water	CEC[(1)] ($cmol_c/Kg$)	V (%)[(2)]	Clay (g/Kg^{-1})	Silt/Clay	T[(3)]
P1	A_1	0–10	7.5YR 3/2	3.8	12.1	12	530	0.35	23
	A_2	10–20	7.5YR 3/2	3.9	8.8	9	527	0.30	17
	A_3	20–40	7.5YR 3/2	4.2	8.1	3	527	0.32	15
	A_4	40–65	7.5YR 4/2	4.5	6.6	7	552	0.22	12
	A_5	65–70	5YR 3/2	4.6	6.3	0	556	0.22	11
	A_6	70–85	5YR 3/2	4.7	6.8	5	494	0.42	14
	A_7	85–95	5YR 3/2	4.7	5.7	0	510	0.26	11
	AB	95–100	5YR 3/3	4.8	5.4	8	535	0.23	10
	BA	100–110	5YR 4/4	4.8	4.8	9	567	0.24	8
	B_1	110–130	5YR 4/6	5.0	4.1	20	541	0.31	8
	B_2	130–170	2.5YR 4/6	5.0	3.7	19	426	0.54	9
	BC	170–200$^+$	5YR 4/6	5.1	3.9	12	303	1.26	13
P2	A_1	0–13	7.5YR 3/2	4.1	10.1	14	543	0.23	19
	A_2	13–26	7.5YR 3/2	4.0	9.2	8	562	0.24	16
	A_3	26–70	7.5YR 3/2	4.2	8.2	5	587	0.17	14
	A_4	70–105	7.5YR 2.5/1	4.3	8.0	4	595	0.11	13
	AB	105–120	7.5YR 3/2	4.3	6.8	4	597	0.16	11
	BA	120–135	7.5YR 3/4	4.4	6.6	8	620	0.10	11
	B_1	135–180	7.5YR 4/6	4.5	4.8	9	652	0.06	7
	B_2	180–210	5YR 4/6	4.7	3.8	9	657	0.07	6
	B_3	210–250	2.5YR 4/6	4.9	3.4	10	641	0.08	5
	B_4	250–320	2.5 YR 4/8	4.7	2.9	10	634	0.09	5
	$2B_5$	320–380	2.5YR 4/6	4.6	4.1	15	428	0.76	9
	2BC	380–450$^+$	5YR 6/8	4.6	4.1	12	276	1.47	15
P3	A_1	0–10	7.5YR 3/2	3.9	16.7	16	373	0.80	45
	A_2	10–42	7.5YR 3/2	4.1	11.0	9	520	0.33	21
	A_3	42–60	7.5YR 3/2	5.1	8.8	13	542	0.28	16
	A_4	60–75	7.5YR 3/2	4.5	7.1	1	546	0.23	13
	A_5	75–94	7.5YR 2.5/1	4.6	6.7	1	577	0.18	12
	A_6	94–101	7.5YR 3/2	4.6	6.2	1	576	0.17	11
	AB	101–118	5YR 3/2	4.7	5.9	9	583	0.16	10
	BA	118–135	5YR 5/6	4.8	4.6	1	606	0.14	8
	B_1	135–165	2.5YR 4/6	4.8	3.7	0	620	0.16	6
	B_2	165–200$^+$	2.5YR 3/6	4.7	3.5	0	654	0.11	5
P4	A_1	0–20	7.5YR 3/2	4.6	9.5	4	531	0.35	18
	A_2	20–50	7.5YR 2.5/1	4.9	7.7	2	505	0.44	15
	A_3	50–60	7.5YR 2.5/1	5.0	6.5	4	581	0.22	11
	AB	60–65	7.5YR3/2	5.0	5.8	7	556	0.31	10
	BA	65–75	7.5YR3/2	5.2	4.8	8	581	0.24	8
	B_1	75–110	7.5YR 4/4	4.9	2.6	1	586	0.17	4
	B_2	110–140	7.5YR 4/6	5.4	2.1	1	669	0.09	3
	B_3	140–180$^+$	5YR 4/6	5.4	2.2	1	691	0.09	3
P5	O	20–0	7.5YR 2.5/1	4.5	13.9	6	174	2.60	80
	A_1	20–35	7.5YR 2.5/1	4.6	12.0	1	126	3.52	96
	A_2	35–60	7.5YR 2.5/1	4.7	9.8	3	252	1.63	39
	A_3	60–80	7.5YR 2.5/1	4.9	9.5	3	349	1.06	27
	A_4	80–90	7.5YR 2.5/1	4.9	8.0	4	177	1.77	45
	AB	90–105	7.5YR 2.5/2	5.0	6.9	4	278	1.09	25
	BA	105–120	7.5YR 3/2	5.2	4.8	6	584	0.12	8
	B_1	120–132	7.5YR 4/4	5.3	3.7	12	568	0.17	7
	B_2	132–175	7.5YR 4/6	5.2	3.2	14	615	0.09	5
	B_3	175–200	5YR 4/6	5.2	2.8	14	633	0.18	4
	B_4	200–250$^+$	2.5YR 4/6	5.2	3.4	12	636	0.20	5

[(1)]CEC: cation exchange capacity;
[(2)]V: base saturation;
[(3)]T: clay activity.

All five soil profiles contained a stone line and its depth which varied between 90 cm and 110 cm featuring a colluvium as cited above in Section 2.1. According to Schaetzl (1998) a stone line in soils within an old landscape, like our study area, can be related to pedogenetic or geomorphic processes such as surface wash, creep, eolian transport, and bioturbation. The contribution of these processes will be discussed in more detail in Section 3.2 according to several proxies that enable identification of LDs.

The clay mineralogy of the studied soil profiles is composed by kaolinite, hydroxy-interlayerd vermiculite, gibbsite, goethite and hematite. We not observed a strong mineralogical difference between superficial and subsuperficial horizons.

The association of a clayey texture (Table 1) and humid conditions (Section 2.1) may indicate microshearing. Microshearing is a result of shrink and swell processes which leads to reorientation of the individual clay plates into planar zones with face-to-face alignment of clay domains (Stoops et al., 2010) and reflects in the field as a shiny surface on peds. This feature was indeed identified with micromorphology and appeared in B horizons of all profiles (Figure 5a and 5b) and is described as a striated b-fabric (pore-striated) by Bullock et al. (1985). B horizon are mainly reddish brown, clayey and have a small size and strong blocky structure breaking into polyhedral, than with the shiny surfaces characterize Nitic horizons (WRB 2015). Some troubles appear to classify those soils with ‘sombric’ horizon as Nitisol because it is not predicted for this class as a qualifier in the WRB classification. Thus we propose here the inclusion of that main qualifier for Nitisol in future updates of WRB. Profiles 1,2,3,4 were classified as Sombric Nitisol humic and profile 5 as a Abruptic Acrisol humic.

In surface horizons and dark subsurface horizons loose discontinuous infillings were observed (Figure 5c and 5d), indicating an intense biological activity in studied soils (Bullock et al., 1985; Silva and Vidal-Torrado, 2001).

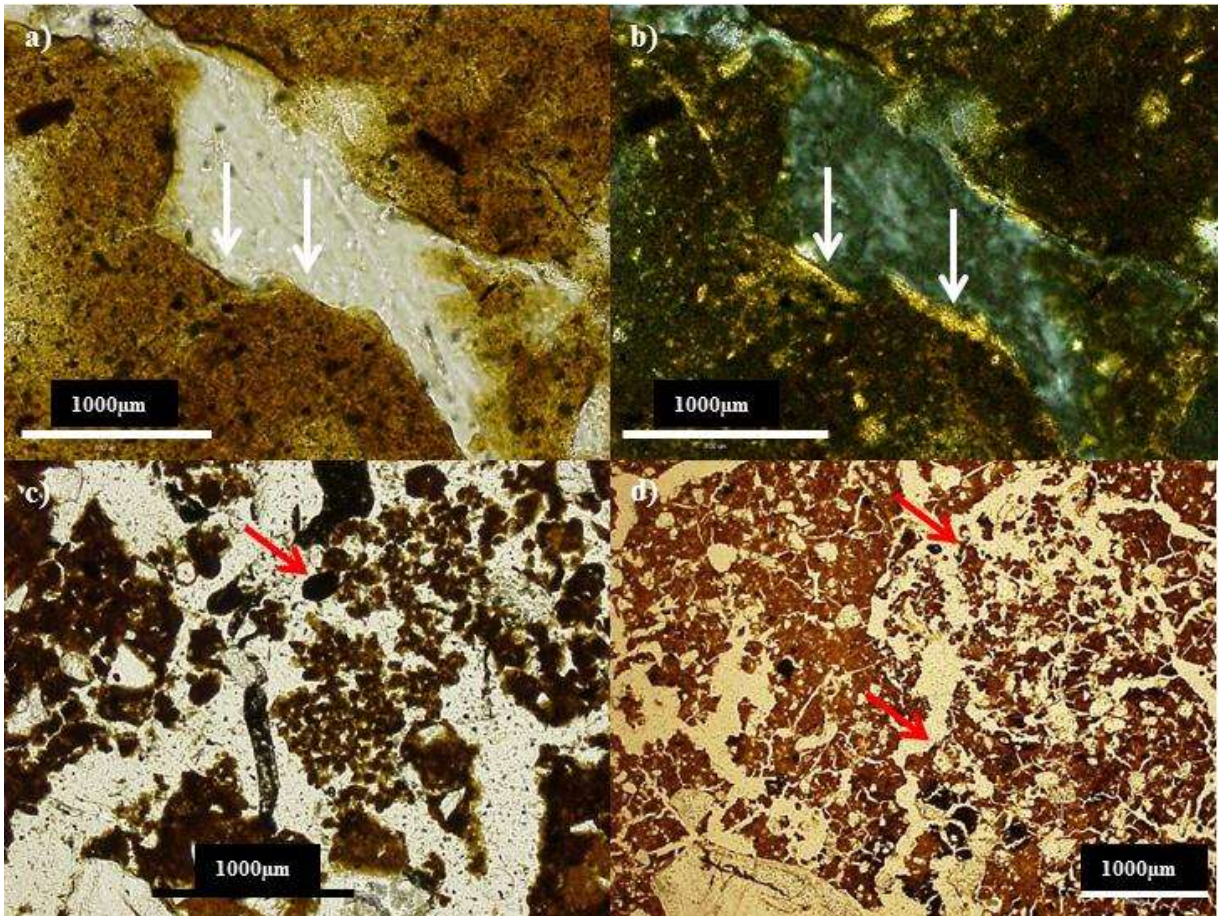

Figure 5. Microshearing in B horizon of P2 (a and b; white arrows); loose discontinuous infillings in A horizons of P3 (c) and P5 (d), indicated by the red arrows.

Microscopic charcoal fragments were observed in the soil matrix of all five profiles (Figure 6a and 6b), which indicates the presence of (past) fires in the area and indicates that black carbon (BC) may have an important influence to the genesis of these dark subsurface horizons. The role of BC will be discussed in more detail in Section 3.6.2.

An interesting characteristic that was observed in the micromorphology analysis was the fact that the organic matter was not concentrated in pores neither in peds (Figure 6c and 6d). However, was observed concentrations of OM in the soil matrix suggesting an interaction between organic matter and the mineral fraction (Almeida et al., 2009), indicating that this dark subsurface horizons (sombric) was not formed by an illuvial process like described by Faivre (1990) and Sys (1961).

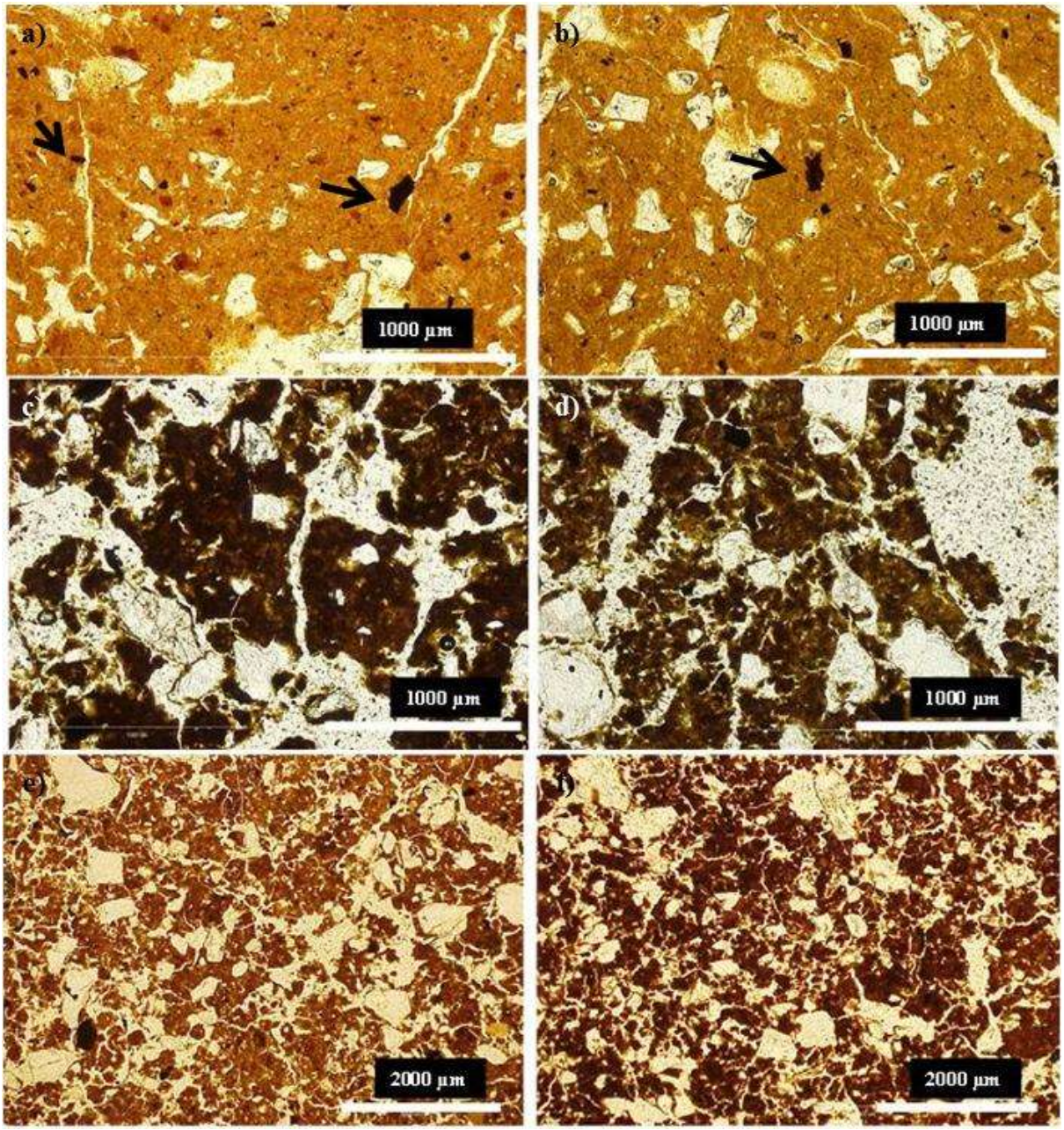

Figure 6. Microscopic charcoal fragments in B horizons (a, b) (black arrows) and organic matter dispersed on soil matrix in dark subsurface horizons of P2 (c) and P3 (d); Difference of soil color matrix in P3 A_3 (e) and P3 A_4 sombric horizon (f).

3.2. Lithologic discontinuities (LDs)

According to Wang and Arnold (1973) the estimates of LDs should be based on various criteria. LDs can be identified based on differences in particle-size fractions (sand/silt ratio and UV indices; Tsai and Chen, 2000), and on an immobile and difficult to weather particle size fraction (Ti/Zr ratio; Tsai and Chen, 2000). Depth records of these parameters are given in Figure 7. The occurrence of LDs in the studied soil profiles is important to

understand the formation of the dark subsurface horizon, because any LD may be indicative for a colluvium. For that reason, the classification of the sombric horizon does not admit the presence of LDs at its upper limit (WRB-FAO, 2014).

Depth records of sand/silt ratio, UV index and Ti/Zr ratio indicate the presence of LDs in all soil profiles (Figure 7). In the soils from the toposequence (P1–P3), LDs occurred at the same depth (100 cm) in the summit (P1), upper backslope (P2) and in lower backslope (P3). For profiles P4 and P5, that are located on another hill, the LD also occurred at 100 cm depth for profile P5 (located at lower backslope). However, for profile P4, that was located at the summit of the hill, the LD was found at about 55 cm depth.

The combination of depth and ^{14}C age for the LDs, in combination with soil morphology and geomorphology, leads some considerations about the 'sombric' and the occurrence of LDs. First, all LDs were found at the base of the 'sombric' horizon (profiles P1–P4), which corresponded to a similar age of about 4000 yrs Cal. BP in profiles that are located at the upper slope (P1, P2 and P4; Table 2), while in profiles P3 and P5, that are located in the lower parts, the age was somewhat younger. This similarity in ^{14}C age at the depth of the LDs probably indicates an event that suggest these soils passed through some creep and erosion event in this area caused by morphoclimatic process (Bigarella et al., 1965). Second, the similar age corresponding to the LDs in profiles P1 – P4, but in different depth of the LD in P4, suggests that the upper part of profile P4 has been eroded, in agreement with its location at the top of the hill. This would imply that profile P4 is not an "intermediate" between soil profile with a 'sombric' horizon (P1– P3) and the reference soil (P5), but reflects a profile with a 'sombric' horizon (similar to P1– P3) from which the upper part has been eroded and on which a newly formed A horizon was superimposed.

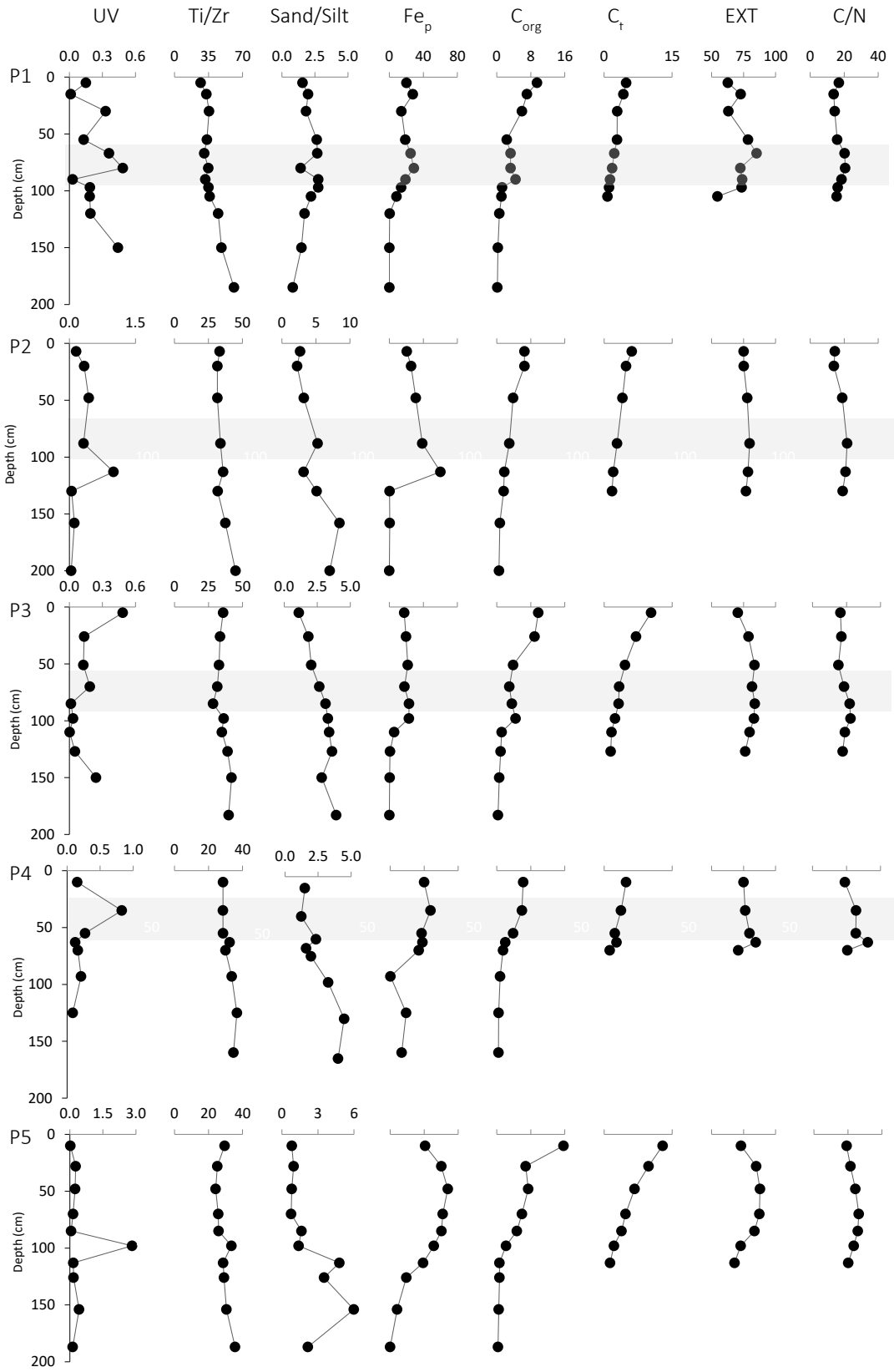

Figure 7. Lithologic discontinuities indexes and some chemical parameters (Vertical axis correspond to depth in cm); UV (uniformity value); Ti/Zr ratio; Sand/silt ratio; Fe_p (g/Kg); C_{org} (g/Kg); C_t (g/Kg) and EXT (%).

Table 2. ^{14}C datings of the study soil profiles.

Pedon	Horizon	Depth (cm)	2 Sigma calibrated age BP	Medium age calibrated BP
P1	A_4	40–65	3923–4085	4004
	A_7	85–95	4809–4850	4829
	B_2	130–170	9515–9557	9536
P2	A_4	70–105	2357–2508	4865
	B_2	180–210	12672–12742	12707
P3	A_3	42–60	2765–2857	2811
	AB	101–118	3463–3579	3521
	B_2	165–200+	10418–10583	10500
P4	A_3	50–60	4528–4657	4592
	B_3	140–180+	13550–13743	13646
P5	A_4	80–90	3718–3872	3795
	B_3	175–200	20083–20460	20271

3.3. Chemical and physical properties

The main chemical and physical properties are listed in Table 1 and Figure 7. The five profiles showed a strong acid reaction, a low base saturation and low cation exchange capacity (CEC). The low CEC go against to the high C content indicating a participation of black carbon in the studied soil profiles.

The total carbon content (C_t) ranged between 0.8 to 12.8 %, and generally showed a decrease with depth in all profiles (Fig. 7; C_t). Furthermore, when C_t contents was compared with Munsell colors (value and chrome), in all studied soils (except P4), the darker colors were accompanied by decreasing C_t contents, similar to Caner et al. (2003) observed in sombric-like subsurface A horizons in Indian soil profiles. On the other hand, the results obtained by Walkley Black analysis of organic carbon (C_{org}) showed an increment of C_{org} in the dark subsurface horizons (Fig. 7; C_{org}). Apart from this general difference, the depth trend showed a relative increase in the dark subsurface horizons of P1 and P3, which was not evident for C_t.

The total carbon content of bulk samples and the distribution of C among the fractions (expressed as percentage) are given in Figure 7. The EXT fraction dominated in all samples with a mean contribution of 77% (with a minimum of 55% and maximum of 88%, compared to 12% and 45% in the RES). The fact that the major part of OM was extractable with NaOH agrees with studied soils of Von Lützow et al. (2007), but was not found for other BC rich tropical soils in which the RES fraction dominated (Justi et al., 2016; Schellekens et

al., 2016). The amount of EXT showed a positive correlation with Fe_p (r^2 = 0.62). The soil profiles of the toposequence (P1–P3) and P4 generally showed an increment of Fe_p with depth and high values were observed in 'sombric' horizons (Section 3.4). The soil profile P5 showed the same tendency. However, this soil profile P5 was the soil that showed the highest values of extractable material. This indicates that the major part of OM that was bound to Fe and Al was extractable with NaOH, and explains the absence of OM in the $Na_4P_2O_7$ extract (Section 2.7.1).

The C/N ratio of bulk samples ranged from 13.9 to 32.5 (Figure 7). All soil profiles showed an increase with depth for C/N until the AB horizons and then decreased again. Furthermore, profiles P1, P2 and P3 showed significantly lower C/N values compared to the reference soil (P5) and the intermediate soil (P4). These lower values suggest that the OM of profiles P1, P2 and P3 was more decomposed than that in P4 and P5 (Knicker, 2008). The maximum C/N values were observed in the dark subsurface horizons from P1–P3 and may be related to BC that has a relatively high quantity of C; this will be further discussed in Section 3.6.2.

3.4. Estimation of Fe and Al forms

The results of Fe and Al forms are given in Table 3. The Fe_d contents showed a clear gradually increase with depth, reflecting the increase of clay with depth (pedogenic iron) (Table 1). This increase with depth was not found for Al_d, which can be related to several sources. First, higher values of Al_d in superficial horizons may be caused by the dithionite-citrate-bicarbonate (DCB) extractions. According to Curi (1983) the successive extractions with DCB (80 °C) is able to dissolve the kaolinite and gibbsite realizing Al^{3+} to extract. The high values of Al_d are most likely due to complexation reactions to sodium citrate catalyzed by high temperature of the extraction procedure (Zhang et al., 1985). Second, and the most important in the superficial horizons and dark subsuperficial horizons high values of Al_d can be related to the extraction of the Al^{3+} that can be arising from isomorphic substitution of Fe^{3+} in the iron oxides.

The amount of Fe_p was substantially higher than that of Al_p, and both showed a positive correlation (r^2 = 0.76). The high values of Fe_p and the high values of the Fe_p/Fe_d ratio suggest that most Fe was in non-crystalline form and were bounded with OM, which is confirmed by the Fe_o/Fe_d ratio. The Fe_o/Fe_d ratio showed generally higher values in the A horizons compared to the B horizons (Table 3). Values of the Fe_o/Fe_d ratio > 0.05 reflect that

the major part of the Fe in the A horizons was in non-crystalline form (Inda Junior and Kämpf, 2003). The large contribution from amorphous Fe in the A horizons can be explained by the relatively high contribution from OM in these horizons, because OM inhibits the formation of crystalline iron oxides (Inda Junior and Kämpf, 2003) and can release iron to OM-metal complexes formation. This is in agreement with the high values of Fe_p that showed that iron was preferentially complexed compared to aluminum. Although the dark subsurface horizons of profiles P1–P3 showed high values of Fe_p and Al_p, profile P5 even showed higher values, thus suggesting that the dark subsurface horizons are not formed by migration of OM-metal complexes associated to clay minerals (Almeida et al., 2009; Faivre 1990). This is confirmed by the absence of clay and OM coatings in micromorphology analysis (Figure 6), and the gradual decrease of C_t with depth (Figure 7).

Table 3. Iron and aluminum analysis in study soil profiles determined with dithionite-citrate-bicarbonate (d), ammonium oxalate (o) and sodium pyrophosphate (p).

Pedon	Hz.	Prof. (cm)	Fe_d (mg/Kg)	Fe_o (mg/Kg)	Fe_p (mg/Kg)	Fe_o/Fe_d	Fe_p/Fe_d	Al_p/Al_d	Al_d (mg/Kg)	Al_o (mg/Kg)	Al_p (mg/Kg)
P1	A_1	0–10	48860	4538	20150	0.093	0.412	0.031	54650	3520	1701
	A_2	10–20	50650	5750	27670	0.114	0.546	0.081	19538	4832	1585
	A_3	20–40	53880	4670	14220	0.087	0.264	0.047	32868	4762	1543
	A_4	40–65	52372	4470	18790	0.085	0.359	0.102	19488	5182	1979
	A_5	65–70	51860	4278	24990	0.082	0.482	0.071	34680	5340	2446
	A_6	70–85	57755	4590	28840	0.079	0.499	0.086	27478	5902	2356
	A_7	85–95	63355	3275	19010	0.052	0.300	0.101	19018	5182	1914
	AB	95–100	68573	2285	13960	0.033	0.204	0.055	24373	4987	1344
	BA	100–110	71371	1537	8380	0.022	0.117	0.039	24710	4810	972
	B_1	110–130	72163	1139	450	0.016	0.006	0.016	15065	4605	244
	B_2	130–170	77894	1107	36	0.014	0.000	0.020	8765	4075	176
	BC	170–200$^+$	77894	666	64	0.009	0.001	0.012	19123	3867	223
P2	A_1	0–13	49500	5320	20550	0.107	0.415	0.114	40135	5765	4583
	A_2	13–26	55280	5350	25610	0.097	0.463	0.134	26720	5660	3576
	A_3	26–70	49595	6355	31100	0.128	0.627	0.153	18005	6455	2758
	A_4	70–105	59410	6820	38750	0.115	0.652	0.073	8735	7135	638
	AB	105–120	59665	7225	60070	0.121	1.007	0.103	44490	6740	4578
	BA	120–135	57285	8055	290	0.141	0.005	0.032	25235	6735	804
	B_1	135–180	64466	2214	487	0.034	0.008	0.039	8013	5187	311
	B_2	180–210	71529	1691	0	0.024	0.000	0.016	19618	4492	321
	B_3	210–250	75004	1796	0	0.024	0.000	0.028	12818	4442	364
	B_4	250–320	80277	1833	15	0.023	0.000	0.044	3381	4040	148
	$2B_5$	320–380	91530	980	11	0.011	0.000	0.027	7868	3712	213
	2BC	380–450$^+$	56382	778	30	0.014	0.001	0.009	26768	3742	254

Table 3. Iron and aluminum analysis in study soil profiles determined with dithionite-citrate-bicarbonate (d), ammonium oxalate (o) and sodium pyrophosphate (p) (Continuing)..

Pedon	Hz.	Prof. (cm)	Fe_d (mg/Kg)	Fe_o (mg/Kg)	Fe_p (mg/Kg)	Fe_o/Fe_d	Fe_p/Fe_d	Al_p/Al_d	Al_d (mg/Kg)	Al_o (mg/Kg)	Al_p (mg/Kg)
P3	A_1	0–10	40745	4975	17530	0.122	0.43	0.076	34353	5677	2607
	A_2	10–42	47022	6898	19640	0.147	0.418	0.523	5508	5912	2878
	A_3	42–60	52535	7485	21710	0.142	0.413	0.824	3674	6217	3028
	A_4	60–75	52465	5965	17850	0.114	0.34	0.171	22353	5957	3818
	A_5	75–94	55615	6975	23190	0.125	0.417	0.253	15510	6100	3931
	A_6	94–101	55002	4958	23000	0.09	0.418	0.213	12838	4512	2731
	AB	101–118	58282	4098	5660	0.07	0.097	0.168	12103	5067	2035
	BA	118–135	57762	2208	780	0.038	0.014	0.234	5614	4135	1311
	B_1	135–165	60235	1685	437	0.028	0.007	0.03	20573	4337	621
	B_2	165–200$^+$	64052	2168	36	0.034	0.001	0.02	23273	4557	455
P4	A_1	0–20	63097	9313	39940	0.148	0.633	0.233	17138	7192	3996
	A_2	20–50	66667	7753	47460	0.116	0.712	0.659	5520	7340	3639
	A_3	50–60	70432	6488	37050	0.092	0.526	0.343	10363	6337	3553
	AB	60–65	70697	7403	37930	0.105	0.537	1.66	1972	6450	3274
	BA	65–75	70607	7283	33680	0.103	0.477	0.531	7018	6632	3730
	B_1	75–110	84902	2148	397	0.025	0.005	0.04	16843	4347	672
	B_2	110–140	97685	2205	18830	0.023	0.193	0.027	16762	6568	455
	B_3	140–180$^+$	97665	3435	13560	0.035	0.139	0.016	28630	4630	453
P5	O	0–20	41175	11375	41150	0.276	0.999	0.128	32558	8792	4170
	A_1	20–35	47102	14108	60160	0.3	1.277	0.038	33553	9857	1282
	A_2	35–60	48782	12318	67770	0.253	1.389	0.04	30350	8480	1221
	A_3	60–80	48675	13805	61850	0.284	1.271	0.156	29443	8417	4599
	A_4	80–90	41267	23153	60350	0.561	1.462	0.062	17200	10670	1072
	AB	90–105	52917	17673	51360	0.334	0.971	0.02	32518	8512	655
	BA	105–120	56542	12698	38780	0.225	0.686	0.126	24603	6427	3106
	B_1	120–132	64005	6075	18990	0.095	0.297	0.04	29093	4327	1162
	B_2	132–175	68307	3403	8250	0.05	0.121	0.043	27715	3525	1185
	B_3	175–200	77977	3393	20	0.044	0	0.028	11770	3150	325
	B_4	200–250$^+$	81740	3370	0	0.041	0	0.025	18853	2647	479

3.5. Selection of vegetation, decomposition and fire parameters

For the paleoenvironmental interpretation of the studied soils, vegetation, decomposition and fire parameters will be selected. The parameters are summed in Table 6, the justification behind their selection will be described below.

3.5.1. Phytoliths

The results of phytolith counts are given in Appendix B, and their morphotypes in Figure 8. The phytolith assembly was dominated by Poaceae morphotypes, and included bilobates, trapeziform polylobate, cross (Panicoid – C_4 grasses), saddle (Chloridoid – C_3/C_4 grasses), rondel (Pooid – C_3 grasses) parallellepipedal bulliform and elongate echinate cuneiform bulliform (Bremond et al., 2008), saddle colapsed (Bambusoid), parallelepipedal echinate bulliform (Bambusoid), cuneiform echinate bulliform (Bambusoid) (Montii et al., 2009). Other species encountered included ferns (Piperno, 1988; Thorn, 2006; Mazumbar , 2011), palm trees (Arecaceae) (Benvenuto et al., 2015; Marcote-Rios et al., 2016) and Araucariaceae (Parr and Watson , 2007) . The identification of these species, in superficial soil samples (0-10cm) is in agreement with the present vegetation composition in the study area, which has been classified as a mosaic of Araucaria forest with grassland (Behling, 2001). The number of phytoliths drastically diminished in the B horizons. In order to correctly compare the data, samples with less than 100 phytoliths were excluded from further analysis, and phytoliths counts were expressed as proportion (%) of the total count of identified phytolith (with taxonomic significance).

A factor analysis was applied to the reduced phytolith data set (FA_{phyt}) in which the total number of phytoliths was also included as a variable. Only the first two factors are considered here. Factor 1 ($F1_{phyt}$) and factor 2 ($F2_{phyt}$) together explained 46.8% of the variance. The factor loadings for each variable are given in Table 4. The morphotypes long cells, which are produced by all subfamilies of Poaceae, and block (from Eudicotyledons) showed high negative loadings on F1, while Panicoid and Chloridoid, both produced by C_4 grasses, showed high positive loadings. Factor 2 separated Pooid (C_3) and Bambusoid (C_4) (negative loadings) from Araucariaceae, Ferns and Panicoid (high positive loadings). Thus factor loadings suggest that $F1_{phyt}$ may reflect a shift between Eudicotyledons (predominantly

shrub) mixed Poaceae vegetation and C_4 grasses (*parameter V1*) with depth, while $F2_{phyt}$ seems to reflect a shift from Araucaria forest/ferns vs. Poaceae (grasses C_4)(*parameter V2*).

Table 4. Factor loadings for phytolith types and the sum of phytoliths.

Family	Phytolith types	F1	F2
	Ferns	0.31	0.69
Poaceae	Panicooid	0.61	0.65
	Pooid	0.44	-0.72
	Chloridoid	0.76	-0.02
	∑ Long cells	-0.60	0.54
	Bulliform	-0.37	-0.46
	Bambusoid	0.18	-0.55
Cyperaceae		0.51	0.17
Arecaceae		0.12	-0.34
Eudicotyledon	Globular	0.53	-0.51
	Irregular	-0.19	-0.01
	Polygonal	-0.57	-0.29
	Block	-0.74	0.18
Araucariaceae		0.23	0.73
Sum		1.23	0.05

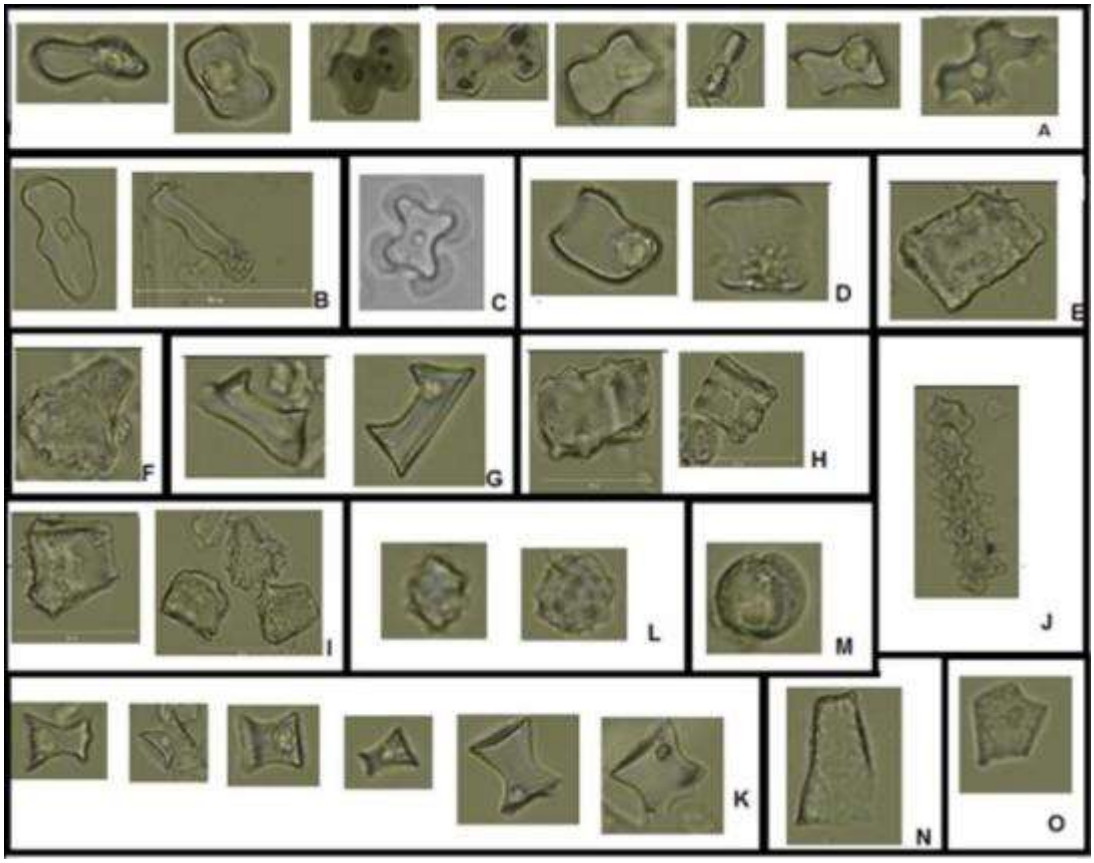

Figure 8. Microphotographs of the main morphotypes found in the studied soil profiles. A) Bilobates; B) Trapeziform polylobate; C) Cross; D) Saddle; E) Parallellepipedal bulliform; F) Cuneiform bulliform; G) Saddle colapsed (Bambusoid); H) Parallelepipedal echinate bulliform (Bambusoid); I) Cuneiform echinate bulliform (Bambusoid); J) elongate echinate; K) Rondel; L) globular echinate (Arecaceae); M) Globular psilate (Eudicotiledonea); N) Polygonal Cell (Eudicotiledonea); O) Hexagonal cyperus (Ciperaceae).

3.5.2. $\delta^{13}C$ isotopic composition

Plants with C_3 photosynthesis cycle (trees, shrub and some grasses) show values of $\delta^{13}C$ that vary from -22‰ to -32‰, while values of C_4 plant species (predominantly grasses) vary between -9‰ and -17‰ (Boutton, 1991; Boutton et al., 1998; Caner et al., 2003; Desjardins et al., 1996). Therefore, depth records of $\delta^{13}C$ (*parameter V3*) can be used to provide information about the vegetation that contributed to the soil profiles. A dominance of C_4 species reflects open vegetation that can be characterized like a grassland or savanna (Victoria et al,. 1995). While dominance of C_3 species can reflect a forest vegetation, here the Araucaria forest (Dümig et al,. 2008).

3.5.3. Molecular composition of soil OM

The pyrograms of the SOM fractions from the studied soil profiles showed a variety of compounds. Our aim was to select parameters that can be used to reflect differences in vegetation, fire and decomposition, both between the profiles and with depth (time). From the different groups of identified compounds the PAHs are well-known pyrolysis products of BC (González-Pérez et al., 2014). The sum of PAHs will therefore be used to reflect the contribution from BC to the SOM (*parameter F1*).

One interesting compound that was identified in soil pyrolysates was totarol, a diterpene compound (Dtp). Totarol is a biomarker for the conifer families Cupressaceae, Podocarpaceae and Araucariaceae (Cox et al., 2007; Schellekens et al., 2013). In the context of the study area, totarol was used to reflect the presence of Araucariaceae (*parameter V4*).

Because most other pyrolysis products can be influenced by several environmental factors, other parameters will be selected using factor analysis that allows observing some tendencies. Factor analysis was applied to all 115 pyrolysis products from both soil OM fractions (FA_{py}) to verify the major chemical differences within the sample set (i.e., soil OM fraction, profile, and horizon or depth). The first two factors explained 62.7%% of the total variance. The distribution of pyrolysis products (loadings) and samples (scores) for the first two factors are plotted against each other in Figure 9. Because factor analysis does not differentiate between products with high or low abundance, mean values of groups of pyrolysis products are provided as well to provide a general idea about the composition of SOM (Table 5).

Table 5. Abundance of groups of pyrolysis products.

Origin or chemical group of pyrolysis products	EXT %	RES %	SD*EXT %	SD* RES %
n-Alkanes	0.61	3.41	0.66	2.20
Branched alkenes	0.98	0.06	1.05	0.08
Alkylbenzenes	0.92	2.51	0.53	0.75
Polyaromatics	2.83	5.96	0.81	1.54
Benzofurans	1.14	1.42	0.23	0.20
Aromatics	19.68	28.38	6.27	4.97
Phenols	6.19	7.10	3.73	4.27
Lignin	1.79	2.12	2.21	2.49
N-compounds	27.0	32.01	3.07	16.99
Polysaccharides	33.16	15.51	7.36	10.30
Aliphatics	5.11	1.46	4.74	0.83
Other	0.58	0.05	1.34	0.09

*Standard deviation

Factor 1 ($F1_{py}$) generally separated EXT (negative scores) from RES (positive scores) samples, with exception of some BA and AB horizons from the RES fraction, that showed slightly negative scores, and A_1 horizons from most profiles in the EXT that showed slightly positive scores (Fig. 9a). Within both fractions, factor 2 (F2) generally separated surface (negative scores) from deeper (positive scores) samples. The EXT samples showed generally higher negative scores for surface samples compared to corresponding RES samples. The loadings demonstrate which compounds correspond to this separation of fractions and depth.

The RES showed the largest contribution from *n*-alkanes, alkylbenzenes and most PAHs and aromatics (high positive loadings on F1). The association of *n*-alkanes with the RES that together accounted for 3.41% of the total quantified products in the RES and 0.61% in EXT agrees with other studies that determined similar soil OM fractions (Lichtfouse et al., 1998; Laird et al., 2001; Wattel-Koekkoek et al., 2001; Grasset et al., 2009; Schellekens et al., 2013, Justi et al., 2016). The contribution from *n*-alkanes was low in relation to these studies because we quantified only part of the n-alkanes (C_{20}–C_{25}). *n*-Alkanes in soils may originate from non-hydrolysable plant polymers (Tegelaar et al., 1995; Nierop et al., 1998), or from microbial aliphatic cell walls that are resistant to biodegradation (Lichtfouse et al., 1998). PAHs accounted for 5.96% of the total quantified products in the RES and 2.83% in EXT. The aromatics and alkylbenzenes (that includes saturated (aB1– aB6; *m*/*z* 91, 92) and unsaturated (aB7– aB11; *m*/z 105,106) alkylbenzenes) accounted for 28.4 % and 2.51 % respectively in the RES and 19.7% and 0.92% respectively in the EXT (Table 5). The

association of aromatics and alkylbenzenes with PAHs indicates a source from BC (Kaal et al., 2008; González-Pérez et al., 2014). A considerable contribution from BC is in agreement with the micromorphology results that were observed the presence of microscopic charcoals.

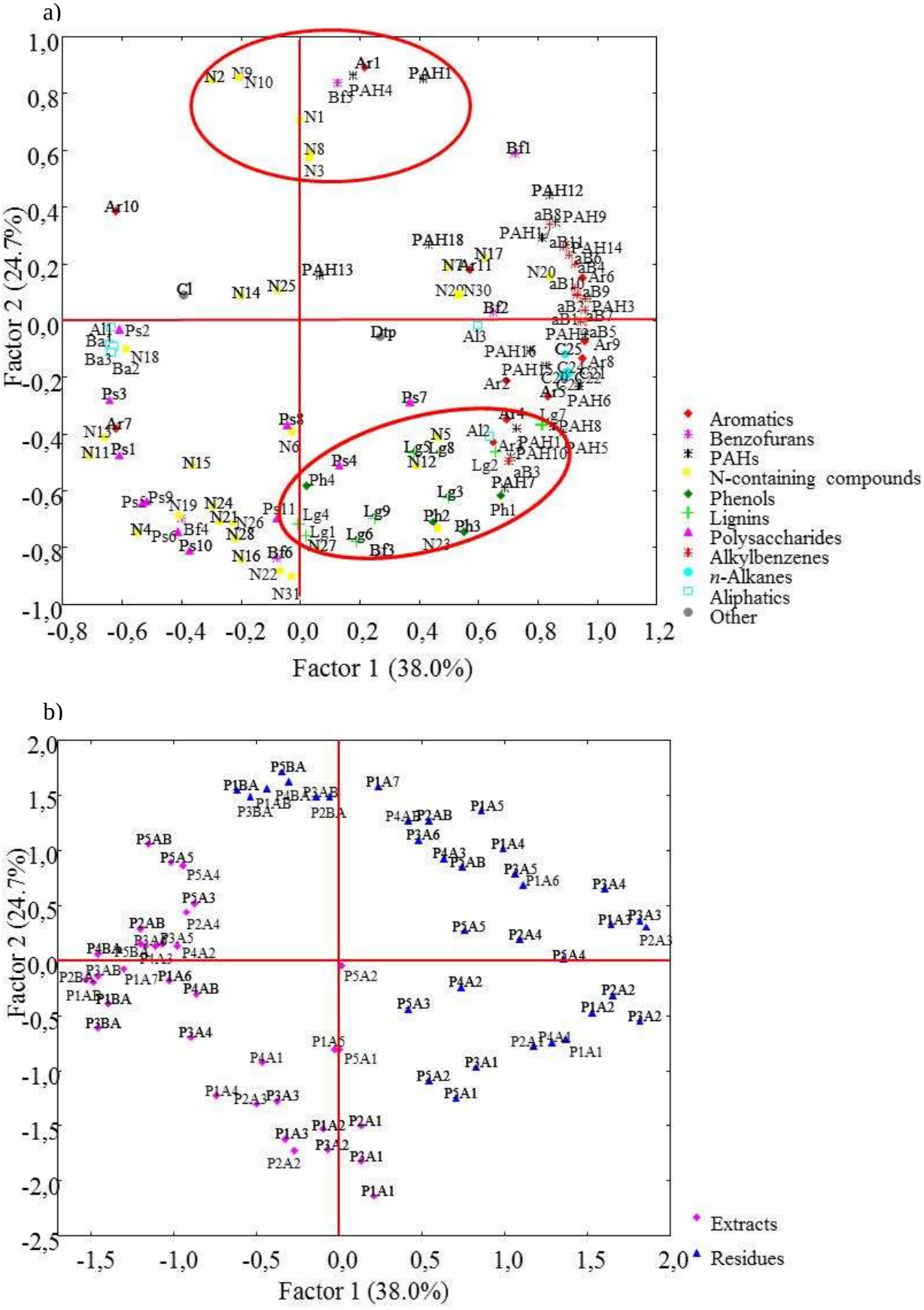

Figure 9. Factor analysis of the pyrolysates products. Factor loadings (a) and scores (b) from soil profiles.

The EXT showed the largest contribution from mainly polysaccharide products which accounted 33.2% of the total quantified products in the EXT and 15.5% in the RES (Table 5). The large contribution from polysaccharides to the EXT fraction was mainly caused by low molecular furan products as is illustrated by the factor loadings (Ps1-Ps3; Figure 9a). In combination with the high negative loadings from 3-methoxypyridine, 2,3,4-trimethylpyrrole, C1 benzonitrile and branched alkenes (BA1, BA2 and BA3) this suggest a dominant microbial source for most polysaccharides (Buurman et al., 2007; Buurman and Roscoe, 2011; Schellekens et al., 2013, 2016).

F2 showed high negative loadings for compounds that are associated with plant materials, including lignin phenols and phenols from lignin and polysaccharides including 4-hydroxy-5,6-dyhydro-(2H)-pyran-2-one (Ps4), 1-deoxy-2,4-methylene-d-xylitol (Ps10) and levoglucosan (Ps11) from (hemi)cellulose (Pouwels et al., 1989; Buurman et al., 2007; Schellekens et al., 2012). Compounds with high positive loadings on F2 included biphenyl (PA4), naphthalene (PA1), dibenzofuran (Bf5), benzene (Ar1), and benzonitrile (N10), all of which are associated with BC and have no functional groups. This association is indicative of degraded BC (Marques et al., 2015; Justi et al., 2016). The fact that products with high negative loadings on F2 were related with plant materials and those high positive loadings with degraded BC suggest that de F2 reflects decomposition with high positive loadings reflecting most resistant SOM. This interpretation is in agreement with the depth trend demonstrated by factor scores. The loadings on F2 can therefore be used to select decomposition parameters, with products with high negative loadings reflecting relatively intact materials and those with high positive loadings reflecting strongly decomposed materials. Lignin phenols (Lg1–Lg8) were more abundant in surface horizons (negative loadings on F2) and are well known that a low contribution in both EXT (1.79%) and RES (2.12 %) indicate a considerable degree of decomposition (Klotzbücher et al., 2011) (*parameter D1*). BC products showed a clear trend on F2, PAHs with alkyl side chain showing more negative loadings and those without alkyl side chain and functional groups higher positive loadings. A loss of alkyl side chains and hydroxyl functional groups from PAHs upon degradation of BC has been reported before (Justi et al., 2016) and is used here as a decomposition parameter, a relatively large contribution from such PAHs reflecting relatively intact BC (*parameter D3*). For the same reason, PAHs without side chains and functional groups (positive loadings on F2) were selected to reflect strongly decomposed BC (*parameter D5*). In addition to BC (PAHs) and plant material (lignin phenols) microbial material is subject to decomposition, which is reflected by shifts of N-containing compounds

on F2. Those with positive loadings are interpreted to reflect more intact microbial material (*parameter D2*), while those with positive loadings are used to reflect microbial material that is strongly decomposed or affected by fire (*parameter D3*).

Table 6. Interpretation of vegetation, fire and decomposition parameters that were selected to interpret environmental conditions. Interpretations refer to high values.

	Parameters	Contents of Parameters	Unit	Environmental Interpretation
Vegetation	V1	$F1_{Phyt}$	-	Decomposition od phytoliths
	V2	$F2_{phyt}$	-	Araucaria forest
	V3	$\delta^{13}C$	‰	C_4 plants
	V4	Totarol (Dtp)	% TIC	(resin) Araucaria forest
Fire	F1	PAHs	% TIC	(BC) Wild fires
Decomposition	D1	Lignin (Lg1, Lg2, Lg3, Lg4, Lg5, Lg6, Lg7, Lg8)	% TIC	relatively undecomposed plant material
	D2	N-containing compounds (N31, N28, N26, N24, N22, N21, N19, N16, N4)	-	Fresh microbial material
	D3	N-containing compounds (N1, N2, N3, N8, N9, N10)	-	Strongly decomposed (microbial) material
	D4	Naphthalenes and naphthalenols with alkyl side chains (PA5-PA8, PA10-PA11)	% PAHs	Undecomposed BC
	D5	PAHs without side chains and functional groups (PA9, PA12, PA15, PA17)	% PAHs	Strongly decomposed BC

3.6. Environmental interpretation

3.6.1. Vegetation composition

Depth records of vegetation parameters are given in Figure 10, and showed generally good agreement between the different proxies, both between profiles and with depth. The biomarker for Araucaria (*parameter V4*) was detected in profiles P4 and P5, and more abundant in the RES compared to the EXT fraction. A larger contribution from Araucaria to P4 and P5 is also evidenced by the phytolith composition, reflected by $F2_{phyt}$ (*parameter V2*). $F2_{phyt}$ showed positive scores for samples from profiles P4 and P5 (except for the sample from 55 cm of depth), and negative scores for those from P1 (except for the sample from 65 cm of depth). Also the $\delta^{13}C$ isotopic composition showed some similarities between P4 and P5, their depth records showed a positive correlation ($r2 = 0.64$) in these profiles, while this was not valid for P1 ($r2 < 0.18$). The $\delta^{13}C$ isotopic composition of soil profile P1, varied between -

25.8 ‰ and -17.9 ‰ in P1, while in P4 and P5 this was between -22.4 ‰ to -15.3 ‰ in P4 and from -26.32 ‰ to -15.67‰ in P5 indicating vegetation sometimes with mixing plant C_3 and C_4 (predominantly C_3 - greater isotopic impoverishment) sometimes composed of plants C_4 (higher isotopic enrichment). However, the $\delta^{13}C$ record showed generally less negative values for P4 and P5, which, contrarily to *parameters V4* and *V2*, imply a lower contribution from trees and a larger contribution from C_4 grasses.

A general observation for most vegetation parameters is that the differences between profiles are larger than those with depth (except for the $\delta^{13}C$ isotopic composition), which suggest that changes in vegetation composition with time were minor compared to lateral differences and the position of pedons in relief. Considering changes with depth, the depth records of vegetation parameters also showed some similarities and differences between the profiles. A clear shift within P1 and P4 coincided with the upper limit of the 'sombric' horizon. In the upper part the $\delta^{13}C$ values were more impoverish indicating a larger contribution from C_3 plants in the vegetation. Furthermore, in both P1 and P4, the $\delta^{13}C$ values showed highest values within the 'sombric' horizon and are in agreement with phytoliths data. In 'sombric' horizon of P1 (~ 60 to100 cm) was observed a predominance of phytoliths of grass and shrubs (79% to 92.9% of the phytolith assembly) Panicoid (C_4) and Chloridoid (C_3/C_4) as well as Bambusoid. The same was observed in P4 (~20 to 90 cm) and the predominance grass (50 % to 100 % of the phytolith assembly) were Panicoid with Bambusoid. Profile P5, however, also showed this depth trend with considerably larger $\delta^{13}C$ values from 30 cm to 85 cm (Panicoid (C_4) e Chloridoid (C_3/C_4) (66.2 % to 92.3 %) and occurrence of Bambusoid and Ferns). So, these observations suggest that the 'sombric' horizons studied here was formed under vegetation composed mainly by C_4 grasses with shrubs during the Medium Holocene (dry and cold conditions). Furthermore, the soil profiles P4 and P5 even showed an isotopic variance greater than 5 ‰, indicating that there was a change in the environmental conditions. The isotopic values and similar vertical variation trends of phytolith assemblage were recorded in soils of Araucaria forest areas by Ewald (2015) in South region of Brazil. According this author the forest began to expand in the upper Holocene to the modern period, evolving into a forest with Araucaria. The Araucaria forest has developed since the upper Holocene (~2.000 yrs Cal. BP), with a humid period and a temperate climate, similar to the present.

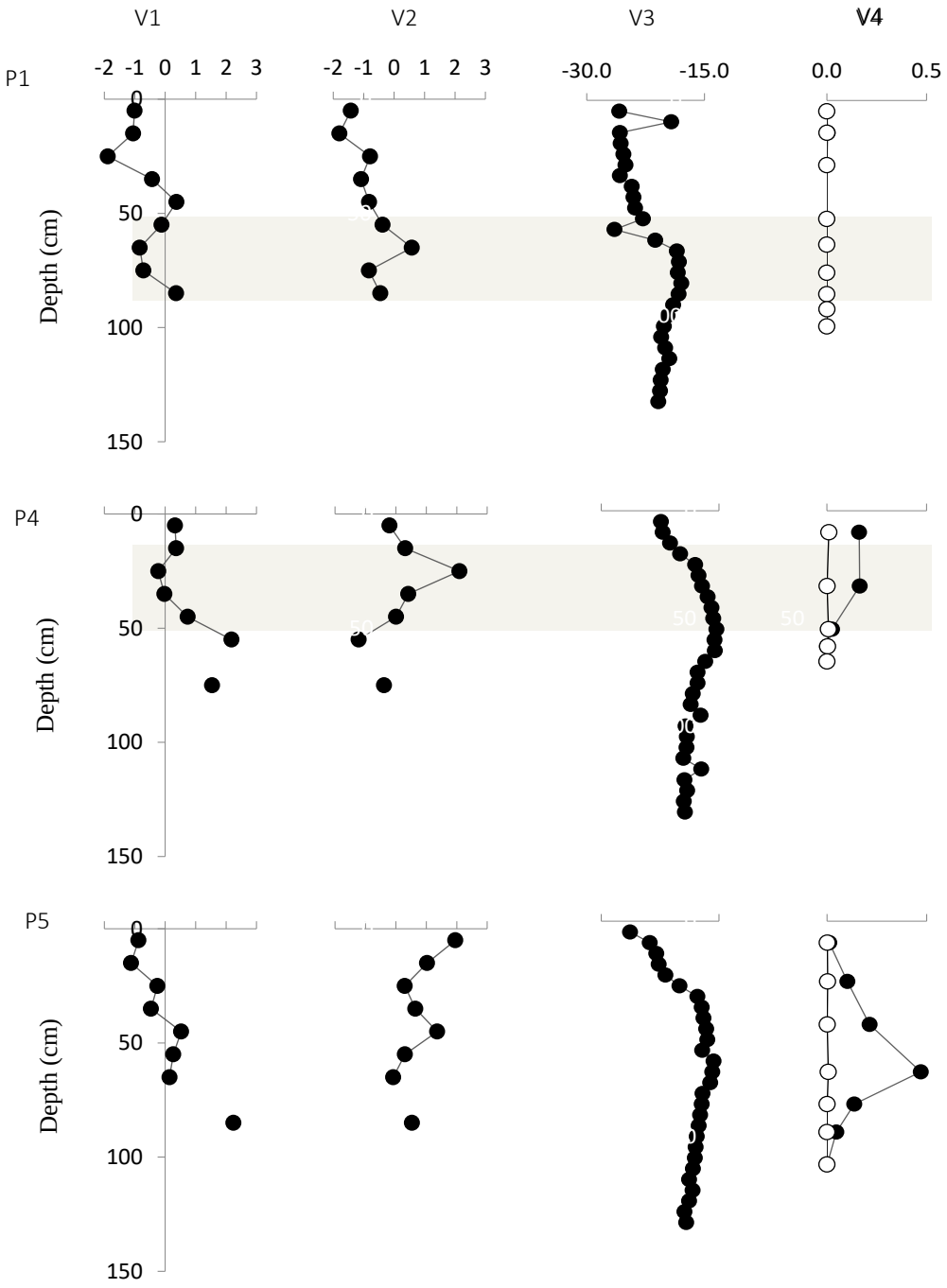

Figure 10. Depth records for selected vegetation parameters (Vertical axis correspond to depth in cm). V1: $F1_{phyt;}$ V2: $F2_{phyt}$; V3: $\delta\ ^{13}C$; V4: Totarol. In V4: Black points represents the RES fraction and white represents the EXT fraction.

3.6.2. BC

The parameter that reflects the contribution from BC is given in Figure 11 (*parameter F1*), and show that the PAHs contributed twice as much in the RES fraction compared to the EXT (Table 5). This difference between the fractions was most obvious in

soil profiles P1 – P3 than P4 and P5 (Section 3.5.3; Figure 11; Appendix C). Profiles P1–P3 showed a clearly larger contribution from PAHs in the RES fraction than P4 and P5. In the RES the PAHs showed a relative increase with depth until the dark subsurface horizons in P1 (from 40 to 85 cm depth), P3 (from 60 to 100 cm depth) and P4 (from 20 to 60 cm depth). Furthermore, this tendency occurs in soil profile P5 that showed an increment with depth until ~70 and 90 cm (Figure 8) decreasing after. This tendency differs from Justi et al. (2016) that observed in Humic Ferralsols under Cerrado a gradual increase with depth of PAHs in the RES fraction.

The more abundance of BC in dark subsurface horizons indicates that these horizons are enriched with them. The enrichment of BC suggests the presence of more fire during the period of formation of 'sombric' horizons as well as a different vegetation composition compared to present. According to the vegetation parameters (Section 3.6.1), during the formation of dark subsurface horizons (P1 – P3) the vegetation was composed predominantly by C_4 grasses with shrubs indicating an open vegetation (Boutton, 1991; Boutton et al., 1998). A more open vegetation corresponds to drier conditions in the study area (Behling, 2001; Dümig et al., 2008;) and thus corresponds with the larger contribution from BC to the 'sombric' horizons. The dominance of shrubs indicates a different size of charcoals (microscopic) in relation that produced by trees (woody; macroscopic charcoal more observed in soil profile P5). This is in agreement with was observed in micromorphology analysis that found microscopic charcoals. In relation to EXT fraction the PAHs showed no depth trend. It can be related to the presence of more degraded and small PAHs compounds and the quickly cycling process of these reactive molecules.

3.6.3. Decomposition

Depth records of molecular decomposition parameters of the five soil profiles are shown in Figure 11. Lignin compounds were observed in low contribution in the fractions (EXT and RES) in all five soil profiles. The general trend in both fractions in all studied soils was a decrease with depth. Profiles P4 and P5 showed some differences compared to profiles P1–P3. First, a different abundance of lignin was observed between EXT and RES in P4 and P5, but not in the other profiles, and this difference between the fractions decreased with depth. Second, the contribution from lignin in P4 and P5 was clearly lower in P4 and P5 in the EXT. The fact that lignin was more abundant in the RES fraction in the upper part of P4 and P5 can be related to the fact that the light fraction was not removed prior to the SOM

fractionation, and thus would be present in RES. This interpretation would imply that P4 and P5 have a larger contribution from litter and conditions are thus less favorable for decomposition compared to P1–P3, which is in agreement with the larger C/N ratio (Figure 7) found in these soil profiles (P4 and P5), thus indicating that SOM in P4 and P5 was less decomposed. A lower degree of decomposition in soil profile P5 is in agreement with the younger age compared with the same depth (~ 80 cm; Medium age of 3795 yr calibrated BP; Table 2), and with the generally low contribution from lignin (in both fractions and all profiles) that indicates a high level of decomposition, because lignin is relatively quickly decomposed by fungi (Klotzbücher et al., 2011).

The decomposition parameters that reflect relatively fresh BC and fresh microbial material showed a similar decrease with depth in the RES fraction in all five soil profiles (*parameters D2* and *D4*), while those that reflect strongly decomposed material showed an opposite trend (*parameters D3* and *D5*). One difference that was observed in relation to soil profile P5 was that the RES showed a larger abundance of fresh BC (*parameter D4*), while in the EXT its contribution was larger for decomposed BC (*parameter D5*) in relation to the other soils. This is in agreement with the interpretation that P5 is generally containing less decomposed material according to lignin and C/N depth records.

The other two decomposition parameters (*parameters D5* and *D3)* showed the same tendency in all five soil profiles for EXT and RES fractions, and both parameters showed a positive correlation in EXT ($r^2 = 0.80$) and in RES ($r^2 = 0.72$). The RES fraction showed an increase with depth of *parameters D3* and *D5*, indicating an enrichment of recalcitrant and more decomposed material (both microbial and BC). This tendency was opposite to that observed from *parameters D1*, *D4* and *D2*. So, with depth was more observed degraded compounds arising from BC and compounds that are enriched with nitrogen.

The EXT fraction showed an increase with depth of *parameters D3* and *D5* until the ‘sombric’ horizon, indicating strongly decomposed microbial material (*D3*) and strongly decomposed BC (*D5*) in P1–P3 and P4 (~ 75 cm) and in soil profile P5 ~ 60 cm depth, thereafter a decrease was observed. For *parameters D4*, *D2* and *D1* this was not observed, even though, *parameters D2* and *D3* showed a negative correlation in the EXT fraction ($r^2 = 0.88$). In other words, in the sombric horizons an increase of N-containing compounds derived by fire (*D3*) corresponds to a decrease of compounds from microbial source that are not altered by fire (*D2*).

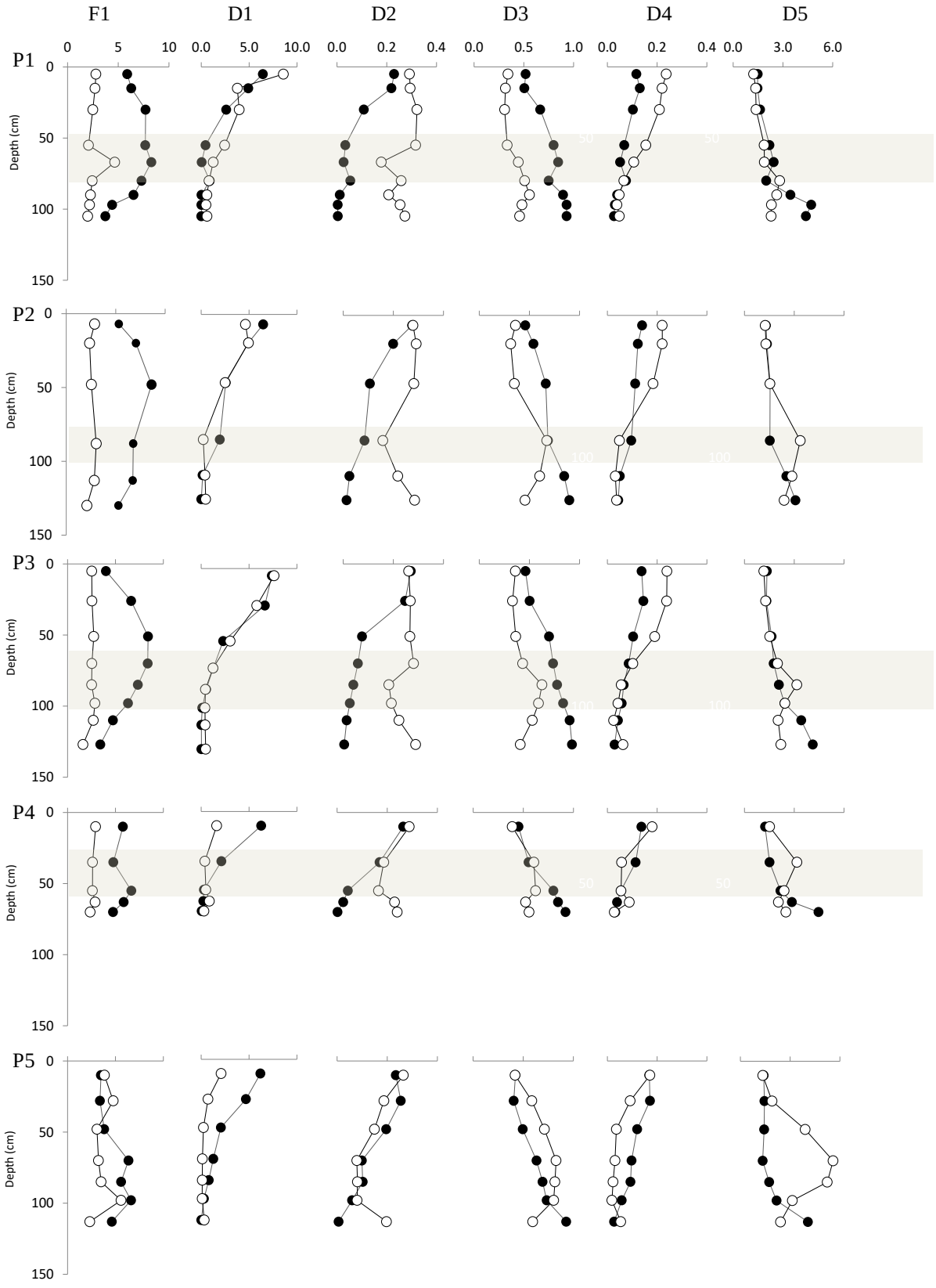

Figure 11. Depth records for selected fire and decomposition parameters (Vertical axis correspond to depth in cm). F1: PAHs compounds; D1: Lignin compounds; D2 and D3:N-containing compounds; D4: Naphthalenes and naphthalenols with alkyl side chains; D5: PAHs without side chains and functional groups. Black points represent the RES fraction and White represents the EXT fraction. (Values in Appendix C).

4. FINAL CONSIDERATIONS

The ‘sombric’ horizons (dark subsurface horizons) studied at Tijucas do Sul (Paraná, Brazil) have been developed during the Mid-Holocene under vegetation composed mainly by C_4 grasses with shrubs. This vegetation was different from that observed at present the latter of which was characterized as an Ombrophilous forest which have significant occurrence of Araucaria trees. The shift from open grassland to ombrophilous forest suggests drier climatic conditions during the formation of the ‘sombric’ horizon compared to present. These dark subsurface horizons can be an expression of the paleoenvironmental conditions in the region.

Micromorphology excluded the possibility that the ‘sombric’ horizon was formed by illuviation of OM, or of OM associated to (clay) minerals. The stability of OM in the ‘sombric’ horizon seemed not related to its association with fine clay, Al and/or Fe. Although a larger contribution from BC was observed in the ‘sombric’, BC was also abundant in other horizons and the reference soil. The BC probably contributed to the maintenance of dark color from the ‘sombric’ horizon in relation to epipedons.

REFERENCES

Almeida, J.A., Cararo, D.C., Uberti, A.A.A., 2009. Genesis of the sombric horizon in Ultisols (Red Argisols) in southern Santa Catarina, Brazil. Revista Brasileira de Ciência do Solo. 33: 405–416.

Almeida, J. A. de, Lunardi Neto, A., Vidal-Torrado, P., 2015. Soil Sombric horizon: five decades without evolution. A review. Scientia agrícola. 72,87–95.

Behling, H., Bauermann, S.G., Neves, P.C., 2001. Holocene environmental changes from the São Francisco de Paula region, southern Brazil. J. South Am. Earth Sci. 14, 631–639.

Benvenuto M. L., Honaine, M. F., Osterrieth, M., Morel, E. M. 2015., Differentiation of globular phytoliths in Arecaceae and other monocotyledons: Morphological description for paleobotanical application. Turkish J. of Botany. 39, 341–353.

Bigarella, J. J. Mousinho, M. R., SILVA J. X., 1965. Pediplanos, Pedimentos e seus depósitos correlativos no Brasil. Boletim Paranaense de Geografia. 16/17, 117–152.

Bin Abas, M.R., Simoneit, B.R.T., Elias, V., Cabral, J.A., Cardoso, J.N., 1995. Composition of higher molecular weight organic matter in smoke aerosol from biomass combustion in Amazonia. Chemosphere. 30, 995–1015.

Boutton, T.W., 1991. Stable carbon isotope ratios of natural materials: II. Atmospheric, terrestrial, marine and freshwater environments. In: Coleman, D.C., Fry, B. (Eds.), Carbon Isotope Techniques. Academic Press, New York, pp. 173–185.

Boutton, T.W., Archer, S.R., Midwood, A.J., Zitzer, S.F., Bol, R., 1998. $\delta^{13}C$ values of soil organic carbon and their use in documenting vegetation change in a subtropical savanna ecosystem. Geoderma. 82, 5–41.

Bremond, L., 2008. Phytolity Indices as Proxies of Grass Subfamilies on East African Tropical Mountains. Global and Planetary Change. 61, 209–224.

Bullock, P., Fedoroff, N., Jongerius, A., Stoops, G. & Tursina,T., 1985. Handbook for soil thin section description. Albrington, Waine Research.

Buurman, P., Peterse, F., Almendros, G., 2007. Soil organic matter chemistry in allophonic soils: a pyrolysis-CG/MS study of a Costa Rica Andosol catena. European J. Soil Sci. Oxford. 58, 1330–1347.

Buurman, P., Roscoe, R., 2011. Different chemical composition of free light, occluded light abd extractable SOM fractions in soils of Cerrado and tilled and untilled fields, Minas Gerais, Brazil: a pyrolysis – GC/MS study. European Journal of Soil Science, Oxford. 62, 253–266.

Calegari, M. R.l., 2013a. Opal Phytolith Extratction in Oxisols. Quaternary International. 287, 56-62.

Caner, L., Toutain, F., Bourgeon, G., Herbillon, A.J., 2003. Occurrence of sombric-like subsurface A horizons in some andic soils of the Nilgiri Hills (Southern India) and their palaeoecological significance. Geoderma 117, 251–265.

Carr, A. S., Boom, A., Chase, B. M., Meadows, M. E., Roberts, Z. E., Britton, M. N.; Cumming, A. M. J., 2013. Biome-scale characterization and differentiation of semi-arid and arid zone soil organic matter compositions using pyrolysis-GC/MS analysis. Geoderma, 200/201, 189–201.

Castro, S.S., Cooper, M., Santos, M.C., Vidal-Torrado, P., 2003. Micromorfologia do solo: bases e aplicações. In: Curi, N., Marques, J.J., Guilherme, L.R.G., Lima, J.M., Lopes, A.S., Alvarez, V.H. Tópicos em ciência do solo. Viçosa: Sociedade Brasileira de Ciência do Solo, 107–164.

Cremeens, D.L., and D.L. Mokma., 1986. Argillic horizon expression and classification in the soils of two Michigan hydrosequences. Soil Sci. Soc. Am. J. 50, 1002–1007.

Cox, R.E., Yamamoto, S., Otto, A., Simoneit, B.R.T., 2007. Oxygenated di- and tricyclic diterpenoids of southern hemisphere conifers. Biochem. Syst. Ecol. 35, 342–362.

Curi, N., 1983. Lithosequence and toposequence of Oxisols from Goias and Minas Gerais State, Brazil, West Lafayette, Purdue University.

Derenne, K. Q., 2015. Analytical pyrolysis as a tool to probe soil organic matter. J. of Analytical and Applied Pyrolysis. 1–37.

Desjardins, T., Carneiro Filho, A., Mariotti, A., Chauvel, A., Girardin, C., 1996. Changes of the Forest–Savanna boundary in the Brazilian Amazonia during the Holocene revealed by stable isotope ratios of soil organic carbon. Oecologia. 108, 749–756.

Dümig, A., Schad, P., Rumpel, C., Dignac, M.F., Kögel-Knabner, I., 2008. Araucaria forest expansion on grassland in the southern Brazilian highlands as revealed by ^{14}C and $\delta^{13}C$ studies. Geoderma. 145, 143–157.

EMPRESA BRASILEIRA DE PESQUISA AGROPECUÁRIA (EMBRAPA). 2011. Manual de métodos de análise de solo. 2.ed. Rio de Janeiro: Embrapa Solos. 230 p.

EMPRESA BRASILEIRA DE PESQUISA AGROPECUÁRIA (EMBRAPA). 2013. Sistema Brasileiro de Classificação de Solos. 3ª ed. Brasília.353 p.

FOOD AND AGRICULTURAL ORGANIZATION – FAO. 2014. World reference base for soil resources Rome. 191p.

Faivre, P., 1990. The sombric horizon: an 'incipient' organic- argillic horizon; the example of soils of the intra-Andean region of Colombia (South America) = L'Horizon sombrique: une ebauche d'horizon organo-argilique; exemple des sols de la region intrandine de Colombie (Amérique du Sud). Pédologie. 40, 273–297.

Frankart, R., 1983. The soils with sombric horizons in Rwanda and Burundi. In: Beinroth, F.H., Neel, H., Eswaran, H. (Eds), Proceedings of the Fourth International Soil Classification Workshop, Rwanda, 1981 – PartI: Papers. ABOS-AGCD, Brussels. pp. 48–64.

Golchin, A., Clarke, P., Baldock, J.A., Higashi, T., Skjemstad, J.O., Oades, J.M., 1997. The effects of vegetation and burning on the chemical composition of soil organic matter in a volcanic ash soil as shown by 13C NMR spectroscopy. I. Whole soil and humic acid fraction. Geoderma. 76, 155–174.

González-Pérez, M., González-Vila, F.J., Almendros, G., Knicker, H., 2004. The effect of fire on soil organic matter – a review. Environment International, New York. 30, 855–870.

González-Pérez, J.A., Almendros, G., De la Rosa, J.M., González-Vila, F.J., 2014. Appraisal of polycyclic aromatic hydrocarbons (PAHs) in environmental matrices by analytical pyrolysis (Py-GC/MS). Journal of Analytical and Applied Pyrolysis. 109,1–8.

Grasset, L., Martinod, J., Plante, A.F., Amblès, A., Chenu, C., Righi, D., 2009. Nature and origin of lipids in clay size fraction of a cultivated soil as revealed using preparative thermochemolysis. Organic Geochemistry, Oxford. 40, 70–78.

Higashi, T., Sakamoto, T., Tamura, K., 1999. Changes in some properties of humic substances from Melanudands induced by vegetational succession from grass to deciduous trees. In: Berthelin, J., Huang, P.M., Bollag, J.M., Hardbound, F.A. (Eds.), Effect of Mineral–Organic–Microorganism Inter-actions on Soil and Freshwater Environments. Kluwer Academic/Plenum Publishers, New York, pp. 203–211.

Inda Junior, A.V., Kämpf, N., 2003. Avaliação de procedimentos de extração dos óxidos de ferro pedogênicos com ditionito-citrato-bicarbonato de sódio. R. Bras. Ci. Solo. 27:1139–1147.

Jackson, M.L., 1979. Soil chemical analysis: advanced course. Madison: By author.

Justi, M., Schellekens, J., Camargo, P. B, Vidal-Torrado, P., Unpublished results. Long-term degradation effects on the molecular composition of black carbono in Brazilian Cerrado soils.

Kaal, J., Martínez Cortizas, A., Eckmeier, E., Costa Casais, M., Santos Estévez, M., Criado Boado, F., 2008. Holocene fire history of black colluvial soils revealed by

pyrolysiseGC/MS: a case study from Campo Lameiro (NW Spain). Journal of Archaeological Science. 35, 2133–2143.

Kaal, J., Martínez Cortizas, A., Nierop K.G.J., 2009. Characterization of aged charcoal using a coil probe pyrolysis-GC/MS method optimized for black carbon. Journal of Analytical and Applied Pyrolysis, Amsterdan., 85, 408–416.

Kämpf, N., Schwertmann, U., 1982. The NaOH concentration method for iron oxides in soils.Clay and Clays Minerals, New York. 30, 401–408.

Klotzbücher, T., Kaiser, K., Guggenberger, G., Gatzek, C., Kalbitz, K., 2011. A new conceptual model for the fate of lignin in decomposing plant litter. Ecology. 92, 1052–1062.

Knicker, H., González-Vila, F.J., Polvillo, O., González, J.A., Almendros, G., 2005a. Fire-induced transformation of C- and N- forms in different organic soil fractions from a Dystric Cambisol under a Mediterranean pine forest (Pinus pinaster). Soil Biology and Biochemistry. 37, 701–718.

Knicker, H., Totsche, K.-U., Almendros, G., González-Vila, F.J., 2005b. Condensation degree of burnt peat and plant residues and the reliability of solid-state VACP MAS 13C NMR spectra obtained from pyrogenic humic material. Organic Geochemistry. 36, 1359–1377.

Knicker, H., Müller, P., Hilscher, A., 2007. How useful is chemical oxidation with dichromate for the determination of "Black Carbon" in fire-affected soils? Geoderma, Amsterdan.142, 178–196.

Knicker, H., 2011. Pyrogenic organic matter in soil: Its origin and occurrence, its chemistry and survival in soil environments. Quaternary International. 243, 251-263.

Laird, D., 2001. Nature of Clay–Humic Complexes in an Agricultural Soil: II. Scanning Electron Microscopy Analysis. Soil Science Society of America Journal, Madison. 65, 1419- 1425.

Leinweber P, Schulten H-R., 2000. Nonhydrolyzable forms of soil organic nitrogen: extractability and composition. J. Plant. Nutr. Soil Sci. 163, 433–439

Lichtfouse, E., Lebond, C., Da Silva, M., Behar, F., 1998. Occurrence of biomarkers and straight-chain biopolymers in humin: implication for the origin of soil organic matter. Naturwissenschaften. 85, 497–501.

Madella, M., Powers-Jones A.H., Jones, M.K., 1998. A Simple method of extraction of Opal Phytoliths from sediments using a non-toxic heavy liquid. Journal of Archeological Science, New York. 25, 801–803.

Madella, M., Alexandre, A., Ball, T., 2005. International Code for Phytolith Nomenclature 1.0. Annals of Botany, Oxford. 96, 253–260.

Mehra, O. P. & Jackson, K. L., 1960. Iron oxide removal from soils and clays by dithionite-citrate system buffered with sodium bicarbonate. In: National Conference on Clay and Clay Minerals, 7, 1958. Proceedings, Washington. 317–327.

Marcote-Ríos, G., Bernal, R., Raz, L., 2016. Phytoliths as a tool for archaeobotanical, palaeobotanical and palaeoecological studies in Amazonian palms. Botanical Journal of the Linnean Society. 182(2), 348–360.

Marques, F.A., Buurman, P., Schellekens, J., Vidal-Torrado, P., 2015. Molecular chemistry in humic Ferralsols from Brazilian Cerrado and forest biomes indicates a major contribution from black carbon in the subsoil. Journal of Analytical and Applied Pyrolysis, Amsterdan. 113, 518–528.

Mazumbar, J., 2011. Phytoliths of pteridophytes. South African Journal of Botany 77(1), 10–19.

Montti, L., Honaine, M.F., Osterriet, M., Ribeiro, D. G., 2009. Phytolith analysis of Chusquea ramosissima Lindm. (Poaceae: Bambusoideae) and associated soils. Quaternary International 193(1), 80–89.

Nierop, K.G.J., Buurman,P., 1998. Composition of soil organic matter and its water-soluble fraction under young vegetation on drift sand, central Netherlands. European Journal of Soil Science, Oxford. 49, 605–615,

Nierop, K.G.J., Van Lagen, B., Buurman,P., 2001. Composition of plant issues and soil organic matter in the first stages of a vegetation sucession. Geoderma, Amsterdan. 100, 1–24.

Nierop, K.G.J., Van Bergen, P.F., Buurman, P., Van Lagen, B., 2005. NaOH and $Na_4P_2O_7$ extractable organic matter in two allophanic volcanic ash soils of the Azores Islandsda pyrolysis GC/MS study.Geoderma. 127, 36–51.

Paisani, J.C., Pontelli, M.E., Corrêa, A.C.B., Rodrigues, R.A.R., 2013b. Pedogeochemistry and micromorphology of oxisols e a basis for understanding etchplanation in the Araucarias Plateau (Southern Brazil) in the Late Quaternary. Journal of South American Earth Sciences. 48, 112.

Parr, J. F., Watson, L., 2007. Morfological characteristics observed in the leaf phytoliths of selected Gymnosperms of eastern Australia. In: MADELLA, M.; ZURRO (Eds), D. Plants, People and Places – recent studies in Phytolith analysis. Oxbow Books.

Pastorova, I., Botto, R.E., Arisz, P.W., 1994. Boon, J.J. Cellulose char structure: a combined analytical Py-GC-MS, FTIR, and NMR study. Carbohydrate Research, Dordercht. 262, 27–47.

Pessenda, L. C. R., 1996. The use of carbon isotopes (13C, 14C) in soil to evaluate vegetation changes during the Holocene in Central Brazil. Radiocarbon. 38(2), 191–201.

Piperno, D.R., 1988. Phytolith Analysis: an Archaeological and Geological Perspective. Academic Press, San Diego.

Pouwels, A.D., Eijkel, G.B., Boon, J.J., 1989. Curie-point pyrolysis high-resolution gas chromatography–mass spectrometry of microcrystalline cellulose. Journal of Analytical and Applyed Pyrolysis, Amsterdan. 14, 237–280.

Santos, L.J.C, Oka-Fiori, C., Canali, N.E., Fiori, A.P., Silveira, C.T., Silva, J.M.F, Ross, J.L.S, 2006. Mapeamento geomorfológico do estado do Paraná. Revista Brasileira de Geomorfologia. 2, 3–12.

Santos, R.D., Lemos, R.C., Santos, H. G., Ker, J. C., Anjos, L. H. C., Shimizu,S. H., 2013. Manual de descrição e coleta de solo no campo. 6.ed. revisada e ampliada. Sociedade Brasileira de Ciência do Solo, Viçosa.

Schatzel, R. J., 1998. Lithologic discontinuities in some soils on drumlins. Theory, detection, and application. Soil Sci. 163, 570–590.

Schellekens, J., Barberá, G.G., Buurman, P., Pérez-Jordà, G.,Martínez-Cortizas, A., 2013b. Soil organic matter dynamics in Mediterranean A-horizons e the use of analytical pyrolysis to ascertain land use history. J. Anal. Appl. Pyrol.104, 287–298,

Schellekens, J., 2013. The use of molecular chemistry (pyrolysis-GC/MS) in the environmental interpretation of peat.Ph.D. thesis, Wageningen University.

Schellekens, J., Almeida-Santos, T., Santana Macedo, R., Buurman P., Kuyper, T.W., Vidal-Torrado, P., 2016. Molecular composition of several soil organic matter fractions from anthropogenic black soils (Terra Preta de Índio) in Amazonia – A pyrolysis-GC/MS study. Geoderma. 288, 154–165.

Schmidt, M.W.I., Skjemstad, J.O., Czimczik, C.I., Glaser, B., Prentice, K.M., Gelinas, Y. & Kuhlbusch, T.A.J., 2001. Compara- tive analysis of black carbon in soils. Global Biogeochemical Cycles. 15, 163–167.

Schoeneberger, P.J., Wysocki, D.A., Benham, E.C., Broderson, W.D., 2002. Field Book for Describing and Sampling Soils, Version 2.0. Natural Resources Conservation Service, National Soil Survey Center, Lincoln.

Schwertmann, U., 1964. Differenzierung der Eisenoxide des Bodens durch Extraktion mit Ammoniumoxalat-Lösung. Zeitschrift für Pflanzenernährung Bodenk. 105,194–202.

Seger, C.D., Dlugosz, F. L., Kuras, G., Martinez, D. T., Ronconi, E., Melo, L. A. N., Bittencourt, S. M., Brand, M. A., Carniatto, I., Galvão, F., Roderjan, C. V., 2005. Levantamento florístico e análise fitossociológica de um remanescente de Floresta Ombrófila Mista localizado no Município de Pinhais, Paraná-Brasil. Floresta. 35 (2), 291–302.

Silva, A.C., Vidal-Torrado, P., 1999. Gênese dos Latossolos Húmicos e sua relação com a evolução da paisagem numa área cratônica do sul de Minas Gerais. Revista Brasileira de Ciência do Solo, Viçosa. 23, 329–341.

Six, J., Conant, R. T., PAUL, E. A., PAUSTIAN, K. Stabilization mechanisms of soil organic matter: Implications for C-saturation of soils Plant and Soil v. 241, p.155-176, 2002.

Soil Survey Staff, 1999. Keys to soil taxonomy.8.ed. Washington, United States Department of Agriculture/Pocahontas Press.

Sollins, P., Homann, P., Caldwell, B.A., 1996. Stabilization and destabilization of soil organic matter: mechanisms and controls. Geoderma. 74,65–105.

Stoops, G., Marcelino, V., Mees, F., 2010. Features related to faunal activity. In:(Ed). Interpretation of micromorphological features of soil and regoliths. Amsterdan. Elservier, 397–414.

Suárez-Abelenda, M., Kaal, J., Camps-Arbestain, M., Knicker, H., Macías, F., 2014. Molecular characteristics of permanganate- and dichromate-oxidation-resistant soil organic matter from a black-C-rich colluvial soil. Soil Res. 52, 164.

Sys, C., Wambecke, A. van, Frankart, R., Gilson, P., Jongen, P., Pécrot, A., Berce, J.M., Jamagne, M., 1961. Soil Cartography in Congo: Principles and Methods = La Cartographie des Sols au Congo: ses Principes et ses Méthodes. National Institute for Agronomy in Belgian Congo. Brussels, Belgium. (Series Science, 66).

Tegelaar, E.W., Hollman, G., Vandervegt, P., de Leeuw, J.W., Holloway, P.J., 1995. Chemical characterization of the periderm tissue of some angiosperm species -recognition of an insoluble. nonhydrolyzable. aliphatic biomacromolecule (suberan). Organic Geochemistry, Oxford,. 23, 239–251.

Tsai, C., Chen, Z., 2000. Lithologic discontinuities in Ultisols along a toposequence in Taiwan. Soil Sci. 165 (7), 587–596.

Thorn, V.C., 2006. Vegetation reconstruction from soil phytoliths, Tongariro National Park, New Zealand. New Zealand Journal of Botany, 44, 397–413.

UNITED STATES DEPARTMENT OF AGRICULTURE – USDA., 1996. Soil survey laboratory methods manual. Version 3.0. Washington, (Soil Survey Investigation Report, 42).

Vancampenhout, K., Schellekens, J., Slaets, J., Hatte, C., Buurman, P., 2016. Fossil redox-conditions influence organic matter composition in loess paleosols. Quaternary international, Oxford. 1–11.

Victoria, R.L., Fernandes, F.,Martinelli, L.A., Cássia Piccolo, M., Camargo, P.B., Trumbore, S., 1995. Past vegetation changes in the Brazilian Pantanal arboreal–grassy savanna ecotone by using carbon isotopes in the soil organic matter. Glob. Chang. Biol. 1, 165–171.

Von Lützow, M., I. Kögel-Knabner, K. Ekschmitt, H. Flessa, G. Guggenberger, E. Matzner, B. Marschner., 2007. SOM fractionation methods: relevance to functional pools and to stabilization mechanisms, Soil Biology and Biochemistry. 39, 2183–2207.

Wang, C. and R.W.Arnold. 1973. Quantifying pedogenesis for soils discontinuities. Soil Sci. Soc. Am. Proc. 37, 271–278.

Wattel-Koekkoek, E. J. W., 2002. Clay associated organic matter in kaolinitic and smectitic soils. Thesis Wageningen University, The Netherlands.

Zhang, Y., Kallay, N. & Matijevic, E., 1985. Interactions of metals hydrous with chelating agents. VII: Hematite-oxalic and citric acid systems. Langmuir. 1, 201–206.

Zegouagh, Y., Derenne, S., Dignac, M.F., Baruiso, E., Mariotti, A., Largeau, C., 2004. Demineralisation of crop soil by mild hydrofluoric acid treatment: influence on organic matter composition and pyrolysis. J. Anal. Appl. Pyrol. 71, 119–135.

APPENDIX

Appendix A. Quantified pyrolysis products of EXT and RES.

Code[a]	**Compound**	***m/z*[b]**	**RT[c]**	**M^{+}[d]**	**Ave. %TIC EXT[e]**	**Ave. %TIC RES[f]**
Ar1	benzene	78	1.842	78	5.092	10.037
Ar2	toluene	91+92	2.517	92	10.096	11.498
Ar3	C_1 benzene	91+106	3.578	106	1.139	1.302
Ar4	C_1 benzene	91+106	3.684	106	1.303	1.514
Ar5	C_2 benzene	91+106	4.029	106	0.867	1.332
Ar6	indene	115+116	6.737	116	0.449	1.604
Ar7	ethanone, 1-(2-methylphenyl)	119+91	6.963	119	0.353	0.081
Ar8	1*H*-indene,1-methyl	129+130	8.807	130	0.143	0.488
Ar9	benzene, 1-methyl-4-(1-propynyl)	129+130	8.946	130	0.133	0.401
Ar10	2-propenal, 3-phenyl	131+78	14.133	132	0.073	0.049
Ar11	unidentified aromatic	173+188	15.875	206	0.036	0.076
Bf1	benzofuran	89+118	5.825	118	0.378	0.631
Bf2	C_1 benzofuran	131+132	8.020	132	0.298	0.348
Bf3	C_2 benzofuran	145+156	10.158	146	0.082	0.062
Bf4	2-coumaranone	78+134	10.575	134	0.091	0.030
Bf5	dibenzofuran	139+168	15.825	168	0.200	0.330
Bf6	unidentified benzofuran	118+161	16.983	-	0.091	0.021
PA1	naphthalene	128	9.558	128	0.925	1.715
PA2	C_1 naphthalene	141+142	11.738	142	0.382	0.803
PA3	C_1 naphthalene	141+142	12.060	142	0.261	0.691
PA4	biphenyl	153+154	13.346	154	0.508	0.841
PA5	C_2 naphthalene	141+156	13.815	156	0.059	0.106
PA6	C_2 naphthalene	141+156	14.103	156	0.057	0.136
PA7	C_2 naphthalene	141+156	14.134	156	0.105	0.132
PA8	C_2 naphthalene	141+156	14.732	156	0.053	0.091
PA9	fluorene	165+166	16.974	166	0.234	0.698
PA10	1-naphthalenol, 2-methyl	129+158	17.525	158	0.011	0.028
PA11	1-naphthalenol, 4-methyl	129+158	17.584	158	0.004	0.012
PA12	anthracene	178	20.142	178	0.099	0.357
PA13	phenanthrene	178	20.252	178	0.087	0.087
PA14	pyrene	202	24.877	202	0.012	0.064
PA15	C_1 pyrene	215+216	26.125	216	0.014	0.052
PA16	benzophenanthrene	226+228	28.992	228	0.006	0.020
PA17	benzo (a) anthracene	226+228	29.075	228	0.005	0.038
PA18	benzo (e) pyrene	252	33.575	252	0.007	0.086
N1	unidentifeid N compound	80+81	2.279	81	1.287	7.784
N2	pyridine	52+79	2.313	79	4.889	5.795
N3	pyrrole	67	2.378	67	2.404	4.487
N4	acetamide	59	2.678	59	3.782	0.561

Appendix A. Quantified pyrolysis products of EXT and RES (Continuation).

Code[a]	Compound	*m/z*[b]	RT[c]	M^{+}[d]	Ave. %TIC EXT[e]	Ave. %TIC RES[f]
N5	C_1 pyridine	66+93	3.007	93	0.860	0.894
N6	C_1 pyrrole	80+81	3.289	81	1.352	1.097
N7	C_1 pyrrole	80+81	3.385	81	0.885	1.258
N8	C_1 pyridine	66+93	3.600	93	1.238	1.531
N9	1*H*-pyrrole, 2,3,5-trimethyl	108	5.308	109	1.727	2.724
N10	benzonitrile	76+103	5.625	103	1.727	2.724
N11	pyridine, 3-methoxy	66+109	5.867	109	0.691	0.135
N12	unidentified N compound	59	5.970		0.081	0.035
N13	2,3,4-trimethylpyrrole	108	6.167	109	0.023	0.023
N14	pyrazine, methoxy	52+110	6.208	110	0.620	0.142
N15	C_1 benzonitrile	90+117	7.642	117	0.209	0.183
N16	4(1*H*)-pyridinone	95	8.200	95	0.468	0.061
N17	3-pyridinol	95	8.484	95	1.042	0.294
N18	C_1 benzonitrile	90+117	8.637	117	0.470	0.689
N19	cinnoline	102+130	9.658	130	0.167	0.069
N20	C_1 cinnoline	78+134	10.517	145	0.090	0.029
N21	quinoline	102+129	10.584	129	0.113	0.205
N22	3-acetamidofuran	83+125	10.618	125	0.587	0.239
N23	2-pyridinecarboxaldehyde	52+79	11.061	107	0.124	0.036
N24	indole	90+117	11.773	117	0.600	0.585
N25	(2-methylpropyl) pyrazine	94+136	15.148	136	0.855	0.022
N26	1-naphthalenecarbonitrile	153+126	15.948	168	0.124	0.116
N27	benzoic acid, 2-(cyanomethyl)	143+161	16.388	161	0.072	0.009
N28	diketodipyrrole	186+93	19.025	186	0.464	0.200
N29	benzimidazole, 2-ethyl-1-propyl	145+92	20.569	188	0.017	0.002
N30	*n*-C_{16} alkylnitrile	110+124	21.725	167	0.020	0.047
N31	*n*-C_{18} alkylnitrile	110+124	24.542	223	0.011	0.034
Ph1	phenol	66+94	5.595	94	4.025	4.767
Ph2	C_1 phenol	107+108	7.500	108	1.863	2.032
Ph3	C_2 phenol	107+122	8.867	122	0.208	0.259
Ph4	catechol	64+110	10.592	110	0.097	0.044
Lg1	guaiacol	109+124	6.121	124	0.800	0.190
Lg2	4-vinylphenol	91+120	10.360	120	0.392	1.169
Lg3	4-vinylguaiacol	135+150	12.129	150	0.249	0.477
Lg4	syringol	139+154	12.850	154	0.076	0.016
Lg5	4-(prop-2-enyl)guaiacol, *trans*	164	14.654	164	0.021	0.056
Lg6	4-acetylguaiacol	151+166	15.373	166	0.195	0.104
Lg7	4-vinylsyringol	165+180	16.688	180	0.024	0.070
Lg8	4-(prop-2-enyl)syringol, *trans*	194	18.900	194	0.006	0.018

Appendix A. Quantified pyrolysis products of EXT and RES (Continuation).

Code[a]	Compound	*m/z*[b]	RT[c]	M[+d]	Ave. %TIC EXT[e]	Ave. %TIC RES[f]
Lg9	4-acetylsyringol	181+196	19.438	196	0.023	0.016
Ps1	2*H*-furan-3-one	54+84	2.777	84	5.226	1.869
Ps2	2-furaldehyde	95+96	3.183	96	14.624	7.386
Ps3	5-methyl-2-furaldehyde	109+110	5.200	110	7.305	2.681
Ps4	4-hydroxy-5,6-dyhydro-(2H)-pyran-2-one	58+114	5.873	114	0.279	0.406
Ps5	unidentified carbohydrate	74+87	10.000	-	0.113	0.014
Ps6	unidentified carbohydrate	74+87	13.625	178	1.251	0.379
Ps7	unidentified carbohydrate	74+87	13.867	-	0.062	0.462
Ps8	unidentified carbohydrate	74+88	13.867	-	0.064	0.050
Ps9	unidentified carbohydrate	101	14.224	-	0.194	0.056
Ps10	1-deoxy-2, 4-methylene-d-xylitol	74+103	14.664	148	0.493	0.119
Ps11	levoglucosan	60+73	15.809	162	3.551	2.088
aB1	n-C5 alkylbenzene	91+92	8.448	134	0.177	0.412
aB2	n-C5 alkylbenzene	91+92	10.678	148	0.174	0.226
aB3	n-C6 alkylbenzene	91+92	11.364	162	0.123	0.363
aB4	n-C7 alkylbenzene	91+92	12.985	176	0.095	0.310
aB5	n-C8alkylbenzene	91+92	14.870	190	0.094	0.309
aB6	n-C9 alkylbenzene	91+92	16.665	204	0.058	0.266
aB7	n-C5 unsaturated alkylbenzene	105+106	9.192	148	0.068	0.206
aB8	n-C6 unsaturated alkylbenzene	105+106	11.175	162	0.044	0.124
aB9	n-C7 unsaturated alkylbenzene	105+106	13.083	176	0.037	0.116
aB10	n-C8 unsaturated alkylbenzene	105+106	14.922	190	0.028	0.095
aB11	n-C9 uinsaturated alkylbenzene	105+106	16.670	204	0.025	0.087
C20	C20 n-alkane	57+71	23.080	282	0.129	0.704
C21	C21n-alkane	57+71	24.408	296	0.120	0.655
C22	C22n-alkane	57+71	25.687	310	0.109	0.628
C23	C23n-alkane	57+71	26.907	324	0.105	0.575
C24	C24n-alkane	57+71	28.073	338	0.074	0.449
C25	C25n-alkane	57+71	29.203	352	0.071	0.399
Al1	branched aliphatic	55+70	3.271	83	4.991	0.981
Al2	pristene	55+56	19.183	-	0.088	0.303
Al3	unidentified aliphatic	81+95	21.812	-	0.035	0.180
BA1	branched alkene	55+69	23.500	-	0.337	0.021
BA2	branched alkene	55+69	26.267	-	0.324	0.024
BA3	branched alkene	55+69	28.792	-	0.322	0.018
Chl	benzene, 1,3- dichloro	146+148	6.113	146	0.579	0.011
Dtp	totarol	271, 286	27.300	286	0.001	0.039

[a] Codes of the chemical groups.
[b] Mass used to quantification.
[c] Retention time.
[d] Molecular weight.
[e] Mean value of the product pyrolysis in EXT.

Appendix B. Detailed counts of phytoliths, recovered from soil samples.

Depth (cm)		Pteridophyta (Fern)	Angiosperm												Gimnosperm	Total Identified
			Monocotyledon								Eudicotyledon					
			Poaceae													
			Panicooid	Pooid	Chloroid	∑Longa cells	Bulliform	Bambusoid	Cyperacea	Arecaceae	Globular	Irregular	Polygonal cell	Block	Araucariaceae	
Perfil 1																
0-10	#	1	11	40	37	37	17	7	0	20	21	0	10	1	0	202
	%	0	5	20	18	18	8	4	0	10	10	0	5	0,5	0	100
10-20	#	0	4	43	13	19	121	60	0	0	10	0	4	4	0	278
	%	0	1	16	5	7	44	22	0	0	4	0	1	1	0	100
20-30	#	0	30	56	50	26	15	13	2	2	23	0	7	0	0	224
	%	0	13	25	22	12	7	6	1	1	10	0	3	0	0	100
30-40	#	0	17	34	41	30	62	1	0	2	8	2	12	0	0	209
	%	0	8	16	20	14	30	1	0	1	4	1	6	0	0	100
40-50	#	0	5	42	9	95	45	0	0	0	7	0	8	0	0	211
	%	0	2	20	4	45	21	0	0	0	3	0	4	0	0	100
50-60	#	0	30	29	26	58	46	2	0	5	5	1	3	3	0	208
	%	0	14	14	13	28	22	1	0	2	2	1	1	1	0	100
60-70	#	1	57	37	60	62	18	9	0	3	5	0	9	2	3	266
	%	0	21	14	23	23	7	3	0	1	2	0	3	1	1	100
70-80	#	0	21	32	44	34	47	9	0	10	7	0	3	2	0	209
	%	0	10	15	21	16	23	4	0	5	3	0	1	1	0	100
80-90	#	0	14	16	42	74	30	0	0	6	7	5	10	14	0	218
	%	0	6	73	19	34	14	0	0	3	3	2	5	6	0	100
90-100	#	0	0	0	0	0	0	0	0	0	0	0	0	0	0	0
	%	0	0	0	0	0	0	0	0	0	0	0	0	0	0	0
100-110	#	0	1	0	1	0	0	0	0	0	1	0	1	0	0	4
	%	0	0	0	0	0	0	0	0	0	0	0	0	0	0	0
110-120	#	0	0	0	0	0	0	0	0	0	0	0	0	0	0	0
	%	0	0	0	0	0	0	0	0	0	0	0	0	0	0	0
120-130	#	0	0	0	0	0	0	0	0	0	0	0	0	0	0	0
	%	0	0	0	0	0	0	0	0	0	0	0	0	0	0	0
130-140	#	0	0	0	0	0	0	0	0	0	0	0	0	0	0	0
	%	0	0	0	0	0	0	0	0	0	0	0	0	0	0	0

Appendix B. Detailed counts of phytoliths, recovered from soil samples (Continuation).

Depth (cm)		Pteridophyta (Fern)	Angiosperm												Gimnosperm	Total Identified
			Monocotyledon								Eudicotyledon					
			Poaceae												Araucariaceae	
			Panicooid	Pooid	Chloroid	∑Longa cells	Bulliform	Bambusoid	Cyperacea	Arecaceae	Globular	Irregular	Polygonal cell	Block		
Perfil 4																
0-10	#	0	14	16	42	74	30	0	0	6	7	5	10	14	2	220
	%	0	6	7	19	34	14	0	0	3	3	2	5	6	1	100
10-20	#	0	42	8	21	87	38	1	0	0	10	0	8	13	1	229
	%	0	18	3	9	38	17	0	0	0	4	0	3	6	0	100
20-30	#	5	51	17	34	80	16	2	2	1	3	1	3	6	6	227
	%	2	22	7	15	35	7	1	1	0	1	0	1	3	3	100
30-40	#	2	32	26	27	105	37	2	0	5	9	2	3	4	2	256
	%	1	13	10	11	41	14	1	0	2	4	1	1	2	1	100
40-50	#	0	21	11	10	121	46	7	0	5	3	1	2	7	0	234
	%	0	9	5	4	52	20	3	0	2	1	0	1	3	0	100
50-60	#	0	1	8	0	33	28	1	0	0	1	0	10	21	0	103
	%	0	1	8	0	32	27	1	0	0	1	0	10	20	0	100
60-70	#	0	1	4	0	8	4	0	0	0	0	0	0	0	0	17
	%	0	6	24	0	47	24	0	0	0	0	0	0	0	0	100
70-80	#	1	12	11	10	87	14	1	0	6	5	0	21	32	0	200
	%	0	4	5	5	44	7	1	0	3	3	0	11	16	0	100
80-90	#	0	0	0	0	1	1	0	0	0	0	0	2	0	0	4
	%	0	0	0	0	0	0	0	0	0	0	0	0	0	0	0
90-100	#	0	0	0	0	0	0	0	0	0	0	0	0	0	0	0
	%	0	0	0	0	0	0	0	0	0	0	0	0	0	0	0
100-110	#	0	0	0	0	0	0	0	0	0	0	0	0	0	0	0
	%	0	0	0	0	0	0	0	0	0	0	0	0	0	0	0
110-120	#	0	0	0	0	0	1	0	1	0	0	0	0	0	0	2
	%	0	0	0	0	0	0	0	0	0	0	0	0	0	0	0
120-130	#	0	0	0	0	3	0	0	0	0	2	0	1	0	0	6
	%	0	0	0	0	0	0	0	0	0	0	0	0	0	0	0
130-140	#	0	0	0	0	0	0	0	0	0	0	0	1	0	0	1
	%	0	0	0	0	0	0	0	0	0	0	0	0	0	0	0

Appendix B. Detailed counts of phytoliths, recovered from soil samples (Continuation).

Depth (cm)		Pteridophyta (Fern)	Angiosperm												Gimnosperm	Total Identified
			Monocotyledon								Eudicotyledon					
			Poaceae													
			Panicooid	Pooid	Chloroid	∑Longa cells	Bulliform	Bambusoid	Cyperacea	Arecaceae	Globular	Irregular	Polygonal cell	Block	Araucariaceae	
Perfil 5																
0-10	#	6	101	19	51	71	18	6	0	1	9	0	2	5	4	293
	%	2	34	6	17	24	6	2	0	0	3	0	1	2	1	100
10-20	#	1	53	14	49	45	40	6	4	2	12	0	1	11	3	241
	%	0	22	6	20	19	17	2	2	1	5	0	0	5	1	100
20-30	#	0	43	20	42	63	55	2	0	0	5	0	0	12	1	243
	%	0	18	8	17	26	23	1	0	0	2	0	0	5	0	100
30-40	#	3	41	29	54	60	18	2	0	0	5	0	3	6	0	221
	%	1	19	13	24	27	8	1	0	0	2	0	1	3	0	100
40-50	#	5	24	12	15	81	36	0	0	5	6	0	0	11	5	200
	%	3	12	6	8	41	18	0	0	3	3	0	0	6	3	100
50-60	#	0	21	14	18	78	51	2	0	2	9	0	4	7	5	211
	%	0	10	7	9	37	24	1	0	1	4	0	2	3	2	100
60-70	#	0	18	17	35	87	41	0	0	4	7	0	0	6	0	215
	%	0	8	8	16	41	19	0	0	2	3	0	0	3	0	100
70-80	#	0	3	1	3	15	10	0	0	0	4	0	0	0	0	36
	%	0	8	3	8	42	28	0	0	0	11	0	0	0	0	100
80-90	#	2	14	2	0	62	12	0	0	3	1	0	3	37	0	136
	%	1	10	1	0	46	9	0	0	2	1	0	2	27	0	100
90-100	#	0	0	0	0	2	1	0	0	0	0	0	0	0	0	3
	%	0	0	0	0	0	0	0	0	0	0	0	0	0	0	0
100-110	#	0	0	0	0	0	0	0	0	0	0	0	1	0	0	1
	%	0	0	0	0	0	0	0	0	0	0	0	0	0	0	0
110-120	#	0	0	0	0	0	0	0	0	0	0	0	0	0	0	0
	%	0	0	0	0	0	0	0	0	0	0	0	0	0	0	0
120-130	#	0	0	0	0	0	0	0	0	0	0	0	0	0	0	0
	%	0	0	0	0	0	0	0	0	0	0	0	0	0	0	0
130-140	#	0	0	0	0	0	0	0	0	0	0	0	0	0	0	0
	%	0	0	0	0	0	0	0	0	0	0	0	0	0	0	0

Appendix C. Fire and decomposition parameters.

			F1		D1		D2		D3		D4		D5	
Pedon	Hz	Depth	EXT	RES	EXT	RES	EXT	RES	EXT	RES	EXT	RES	EXT	RES
P1	A1	0-10	2.80	5.89	8.58	6.44	0.29	0.23	0.34	0.52	0.24	0.12	1.23	1.48
	A2	10-20	2.71	6.28	3.77	4.91	0.29	0.22	0.32	0.51	0.22	0.13	1.36	1.47
	A3	20-40	2.49	7.69	3.96	2.61	0.32	0.11	0.31	0.67	0.21	0.10	1.38	1.63
	A4	40-65	2.07	7.67	2.44	0.45	0.32	0.03	0.33	0.80	0.15	0.07	1.87	2.19
	A5	65-70	4.65	8.26	1.25	0.05	0.18	0.03	0.45	0.85	0.11	0.05	1.88	2.44
	A6	70-85	2.43	7.30	0.81	0.89	0.26	0.05	0.51	0.75	0.07	0.08	2.80	1.99
	A7	85-95	2.26	6.50	0.59	0.03	0.21	0.01	0.56	0.90	0.05	0.04	2.63	3.45
	AB1	95-100	2.17	4.40	0.50	0.01	0.25	0.00	0.48	0.93	0.04	0.03	2.31	4.71
	BA	100-110	1.98	3.73	0.60	0.01	0.27	0.00	0.46	0.93	0.05	0.03	2.29	4.39
P2	A1	0-13	2.87	5.33	4.63	6.48	0.28	0.28	0.36	0.46	0.22	0.14	1.25	1.29
	A2	13-26	2.36	7.05	4.94	4.92	0.29	0.20	0.31	0.54	0.22	0.12	1.30	1.36
	A3	26-70	2.55	8.62	2.51	2.56	0.28	0.11	0.35	0.66	0.18	0.11	1.54	1.55
	A4	70-105	3.03	6.78	0.22	1.95	0.16	0.09	0.67	0.68	0.05	0.10	3.36	1.53
	AB	105-120	2.84	6.73	0.40	0.15	0.22	0.03	0.60	0.85	0.03	0.05	2.87	2.53
	BA	120-135	2.09	5.28	0.47	0.02	0.28	0.01	0.46	0.90	0.04	0.04	2.39	3.08
P3	A1	0-10	2.52	4.01	7.62	7.38	0.26	0.27	0.36	0.46	0.24	0.14	1.17	1.35
	A2	10-42	2.55	6.64	5.81	6.65	0.27	0.25	0.33	0.50	0.24	0.14	1.27	1.33
	A3	42-60	2.74	8.40	3.03	2.30	0.27	0.08	0.36	0.70	0.19	0.10	1.52	1.64
	A4	60-75	2.54	8.36	1.24	1.26	0.28	0.06	0.43	0.74	0.10	0.09	1.99	1.76
	A5	75-94	2.51	7.35	0.45	0.52	0.18	0.04	0.63	0.78	0.06	0.07	3.16	2.08
	A6	94-101	2.85	6.31	0.40	0.12	0.19	0.03	0.59	0.84	0.04	0.06	2.44	2.41
	AB	101-118	2.69	4.73	0.42	0.03	0.22	0.01	0.53	0.90	0.03	0.04	2.03	3.42
	BA	118-135	1.61	3.42	0.47	0.03	0.29	0.00	0.41	0.92	0.06	0.03	2.20	4.12

Appendix C. Fire and decomposition parameters (Continuation).

			F1		D1		D2		D3		D4		D5	
Pedon	Hz	Depth	EXT	RES	EXT	RES	EXT	RES	EXT	RES	EXT	RES	EXT	RES
P4	A1	0-20	2.93	5.78	1.63	6.28	0.29	0.26	0.39	0.45	0.18	0.14	1.52	1.24
	A2	20-50	2.61	4.78	0.38	2.12	0.19	0.17	0.61	0.55	0.06	0.11	3.16	1.52
	A3	50-60	2.60	6.66	0.49	0.30	0.17	0.04	0.62	0.80	0.05	0.05	2.39	2.17
	AB	60-65	2.88	5.86	0.86	0.23	0.23	0.02	0.52	0.85	0.09	0.04	2.05	2.86
	BA	65-75	2.36	4.75	0.29	0.06	0.24	0.00	0.56	0.92	0.03	0.03	2.50	4.46
P5	O	0-20	3.85	3.48	2.08	6.19	0.26	0.23	0.42	0.42	0.17	0.17	1.35	1.41
	A1	20-35	4.77	3.39	0.72	4.68	0.19	0.25	0.59	0.41	0.09	0.17	1.91	1.45
	A2	35-60	3.07	3.83	0.24	2.06	0.15	0.20	0.71	0.50	0.04	0.12	3.91	1.43
	A3	60-80	3.23	6.36	0.13	1.27	0.08	0.10	0.83	0.63	0.03	0.10	5.59	1.35
	A4	80-90	3.50	5.59	0.12	0.80	0.08	0.10	0.82	0.69	0.02	0.09	5.24	1.74
	AB	90-105	5.59	6.63	0.11	0.30	0.08	0.06	0.80	0.73	0.02	0.06	3.14	2.18
	BA	105-120	2.32	4.62	0.32	0.01	0.20	0.01	0.59	0.93	0.05	0.03	2.42	4.07